The Contribution of Synchrotron X-ray Powder Diffraction to Modern Zeolite Applications: A Mini-review and Future Prospects

Benedict Tsz Woon Lo[1,2†], Lin Ye[1†], Shik Chi Edman Tsang[1,2*]

[1]Wolfson Catalysis Centre, Department of Chemistry, University of Oxford, OX1 3QR, UK
[2]Department of Applied Biology and Chemical Technology, Hong Kong Polytechnic University, Hong Kong, China
†These authors contributed equally.
*Email: edman.tsang@chem.ox.ac.uk

Shik Chi Edman Tsang will be served as the Lead Contact.

Summary

Synchrotron X-ray powder diffraction has begun to stretch its strategic presence from the sheer determination of crystal structures into the mechanistic and kinetic information of microporous zeolite materials. Not only can this technique be used to reveal the internal framework structure of zeolites and their active sites, but it can also be combined with other analytical tools to suit the particular needs for *in situ* or *operando* gas storage/separation and catalytic studies. This review covers the recent development of using synchrotron X-ray powder diffraction as the primary tool for the study of fundamental interactions with organic molecules with active sites in powder zeolites, and some perspectives based on this new experimental capability.

1. Introduction

Silicate in origin, zeolites occur naturally or can be synthesised commercially. As of July 2017, there are 235 unique zeolite frameworks reported in the literature, with their framework codes approved by the International Zeolite Association. The most value-added application of zeolites is in the petroleum refining and catalysis industries. The most industrially important zeolites are: A (a commercial drying and gas separation agent), X and Y (mainly used in fluid catalytic cracking (FCC)) and ZSM-5 (important for xylene isomerisation, disproportionation of toluene, production of crude-oil-derived hydrocarbons, such as the methanol-to-hydrocarbons (MTH), methanol-to-gasoline (MTG) and methanol-to-aromatics (MTA)).[1]

Zeolites are composed of interconnecting TO_4 (where T = Si or Al) tetrahedra, connected via the corner O atoms. The tetrahedra form distinct three-dimensional structures dependent on synthesis, substrate composition and reaction conditions. They are microporous materials that possess pores (or channels) ranging from 3 Å (zeolite A) to 13 Å (zeolite Y), see Figure 1. When tetravalent Si(IV) is substituted with trivalent Al(III), charge imbalance is created and then compensated by cations (e.g. H^+ and Na^+). In the H^+-form, an H^+ moves close to the O atoms bonded to the substituted Al atom to form a Brønsted acid site (BAS). In principle, this H^+ can be populated on any one of the four O atoms bonded to each framework-Al site, as demonstrated in the early work by Haag et al.[2] These substituted sites are found to be synthesis condition dependent, where control measures, like the use of organic templates, have been employed to alter the location of substitution sites.[3] The H^+ of BAS, when exchanged with transition metal cations, may serve as Lewis acid/basic sites (LAS/LBS) of different strengths.

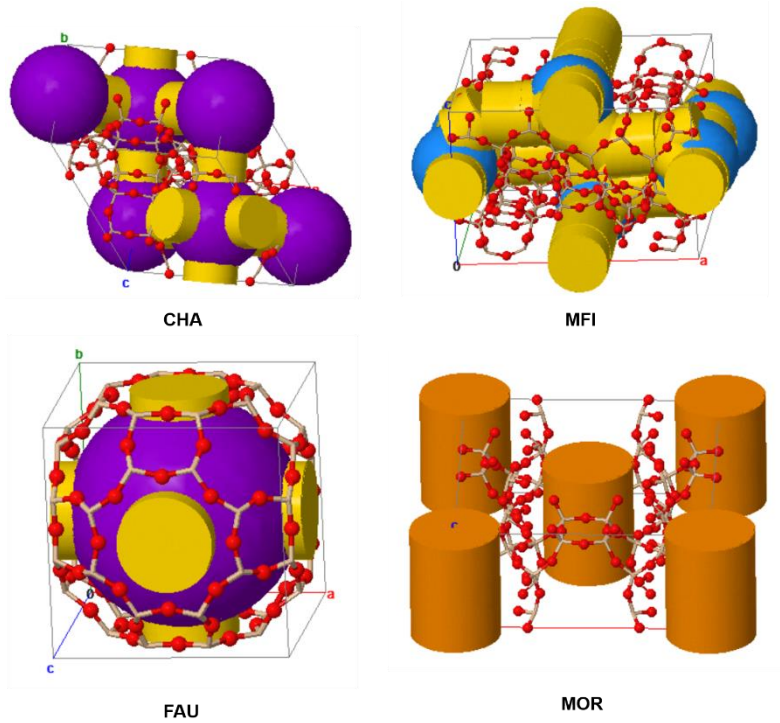

Figure 1. Some typical zeolites showing their vertices and channels. The images are generated from the ZEOMICS method developed by Gounaris et al.[4] Ball-and-stick model: red = O, and yellow = Si/Al.

The unique chemical/physical properties of zeolites in adsorption, gas separation and catalysis, are caused by their microporous framework structures and inherent surface Brønsted and Lewis acidities. There are a lot of well-studied zeolite characterisation techniques[5], such as calorimetry, Fourier transform-infrared (FT-IR) spectroscopy with or without probe molecules, thermogravimetric analysis (TGA), temperature programmed desorption (TPD) with basic probe molecules, solid-state nuclear magnetic resonance (ssNMR) spectroscopy, etc.

The acidic properties are not the full story of zeolite chemistry, where the structural properties of zeolites may often complete the remaining half by offering unique spatial features. The pore shape and size determine which molecules can enter the zeolite frameworks, and how the pore hinders the product distribution in catalytic reactions. However, traditional characterisation techniques do not provide sufficient structural information of the acidic sites in spatial resolution, or their corresponding structural chemistry in zeolites. Classically, shape and size selectivities are understood to be caused by mass transfer (molecular diffusion) and transition state (the configuration of the transition state) effects.[6] The former circumvents merely the formation or diffusion of 'over-sized' products by the rigid zeolite framework, acting as a molecular sieve. The latter is caused by the confined space within the zeolite framework that influences the formation of individual transition state species.

For studying the topological structure of zeolites, X-ray diffraction (XRD) has long been regarded as an indispensable crystallographic technique based on Bragg's law. Historically, many crystal structures of earlier reported zeolites, including both naturally occurring and synthetic zeolites have been solved by XRD using single-crystal samples (which will be described later). One of the first crystal structures solved was zeolite A, reported by Reed and Breck in 1956.[7] The channel dimensions and the probable cationic sites of zeolite A regarding atomic coordinates were also reported. Since then, following the development of zeolites as petrochemical catalysts, an increasing number of synthetic zeolites has been prepared and characterised. Synthetic mordenite is widely used as an adsorbent and for the catalytic isomerisation of alkanes and aromatics.[8] The crystal structure of a natural mordenite sample exchanged with Na^+ was first reported by Meier in 1961 using single-crystal XRD.[9] Faujasite is another important

class of zeolites in catalysis, which is mainly used for the catalytic cracking of long-chain hydrocarbons into gasoline. The crystal structure of faujasite was solved by Olson et al. in 1969 by single-crystal XRD.[10] Furthermore, the crystal structure of ZSM-5, another class of industrially significant zeolite in catalysis, was solved by Olson et al. in 1978.[11]

In the early days, the crystal structures of most zeolites were mostly solved by single-crystal XRD rather than by powder XRD (PXRD). However, the single-crystals of many zeolites are challenging to grow, due to some intrinsic structural problems, for instance, the presence of pseudosymmetry, intergrowth and disordered structures.[12] Aside from the long-discussed intergrowth structures of ZSM-5/ZSM-11[13, 14], recent structural studies are reported on the intergrowth structures of one phase on the other using Rietveld refinement of mixed phases in the cases of SAPO-18/34[15] and CHA/AEL[16]. Even today, the determination of crystal structures using powder samples is not as straightforward as it is for single-crystals. It is mainly due to a much greater number of experimental observables (*hkl* reflections) from a three-dimensional single-crystal XRD pattern than that from a summed one-dimensional PXRD pattern. From the statistical point of view, an accurate and reliable refinement requires a much greater number of experimental observables than refinement parameters. As the incidental effects due to the very close lattice parameters may lead to severe peak overlap, high-resolution diffraction data – especially when using synchrotron X-rays – is necessary for high-quality structure refinement. On the other hand, PXRD is more relevant to the applications in zeolites, as powder materials are commonly used in industry.

Synchrotron X-rays are generated by large particle accelerators where high-speed electrons (approaching the speed of light) are accelerated in magnetic lattices such as bending magnets and insertion devices (undulators and wigglers). There are many powerful synchrotron X-ray sources, especially at today's 3rd generation synchrotron facilities such as Diamond Light Source ('Diamond', UK), European Synchrotron Radiation Facility (ESRF, France), Advanced Photon Source (APS, USA) and SPring-8 (Japan), etc. Detector development is also a crucial factor. Currently, the 'zero-background' Pilatus detector (Dectris) is broadly used. It detects the electrical signal converted from the incoming X-ray photons based on the photoelectric effect.[17] The Pilatus detector possesses a high dynamic range whilst retaining high sensitivity. It can even allow studies with spatial resolution down to a few microns. Synchrotron X-ray powder diffraction (SXRD) is known to be outstanding when compared with the laboratory analogues, by taking advantage of the unique properties of synchrotron X-ray beam listed below[18]:

- Higher brilliance (intense and tight collimation) means: (i) smaller angular divergence of the beam, hence high angular resolution data can be obtained, and (ii) deep probing of structural details with high contrast (high signal-to-noise ratio) data for the detection of small features,
- Horizontally polarised, which reduces the fall in intensity as a function of 2θ,
- Tuneable X-ray wavelength, i.e. the X-ray absorption problems of individual atoms can be avoided, which reduces sample fluorescence that causes high background,
- A large or spacious instrument for different sample environments, and
- Faster data acquisition.

Thanks to the recent development of the insertion devices (undulators and wigglers), very high brilliance beamlines (beyond storage beam emission) have been constructed for hard X-ray (typically at energy > 30 keV) measurements. With more relevance to the dynamic study of catalysis chemistry, hard synchrotron X-rays can be beneficial for *in situ/operando* PXRD studies[19]:

- Higher penetration depths, which allows the use of a much larger experimental reactor, such as an industrial tubular reactor, thus improving realism,
- Lower radiation damage, due to a reduction of ionising electrons from photoelectric effect, and
- More suitable for two-dimensional Pilatus area detector, due to the flattening of the Ewald sphere. This allows much faster data acquisition when compared with any other point (one-dimensional) detector.

However, a reduction in angular resolution may be resulted due to the collapse of Bragg's peaks. Researchers should therefore thoroughly consider the balance between the benefits and limitations when using hard synchrotron X-rays for PXRD studies.

Indeed, the advent of high brilliance 4th generation synchrotron X-ray sources (a.k.a. X-ray free-electron lasers (XFEL)) has been sought to be a potential tool in conducting zeolite catalysis studies. Specially designed XFEL beamlines for PXRD experiments have been built. A notable example is BL3 of SCALA (Japan), where a coherent pulse in the range of 4.5-19.5 keV contains photons in the order 10^{11} and has a temporal width of 10 femtosecond.[20] Ultrafast dynamics of catalysis chemistry can be probed. However, two major problems, namely sample stability and selective triggering, due to the intrinsic properties of high energy and brilliance X-ray need to be first tackled, before the real application of PXRD using XFEL source for heterogeneous catalysis studies. Jacinto Sá and Jakub Szlachetko have explicitly warned that XFEL experiments are inherently different from those at synchrotron X-rays.[21] Hence, similar experiments using synchrotron X-ray should not be considered as a pre-run for work at XFEL.

SXRD has been employed in many research areas (e.g. gas storage/separation and catalysis) related to zeolite. This review covers areas mainly for the beginners, which includes the spatial determination of active sites, the atomic level interaction between gas molecules and active sites over pure or modified zeolites, etc. Owing to the recent development of synchrotron X-ray facilities around the globe, researchers have started to apply SXRD with Rietveld refinement to determine various properties of powder zeolite materials. Rietveld refinement is a whole-pattern fitting method using a non-linear least-squares procedure.[22] It minimises the quantity based on the calculated peak intensity and observed peak intensity, with applied weighting statistics. The Rietveld refinement allows simultaneous refinements and adjustments of the structural parameters against the proposed structural model. The fractional atomic coordinates (x, y, z), site occupancy factors (SOF), and atomic displacement parameters (ADP, often incorrectly called as the temperature factor) of the framework atoms of zeolites can be obtained.[22] In addition to the atomic parameters, other information could also be obtained from XRD, such as topology, 'apparent' crystal size, strain or stress, the extent of heteroatom substitution and crystallinity (e.g. lattice imperfections, stacking faults, dislocation and atomic species disorder).[5] Like other curve/peak fitting techniques, a set of R-factors can be used to evaluate the quality and progress of Rietveld refinement.[23] However, before judging the quality of the fit, the investigator should first study how close the fitting is between the observed and calculated PXRD pattern. This means that the difference plots should be first examined to identify any gross errors in the structural model. For a well-fitted PXRD pattern, the difference between the observed and calculated patterns should be small, and no specific peaks should be poorly fitted. If there is any major peak discrepancy, it may suggest a presence of faults in the proposed model. Finally, and equally importantly, the chemistry of the atomic parameters, such as the derived bond distances, derived bond angles, and SOF, must be reasonable. The refined result would still make no sense without arriving at a sensible and reasonable final crystal structure, even if the R_{wp} (weighted profile R-factor) value is low. David[24] and Toby[25] have independently discussed the meanings of the fitting quantities of Rietveld refinements. It is proposed that adequate refinements have R_{wp} below 12%, and χ^2 should approach 1 for a perfect refinement. Lutterotti and Scardi[26] have also critically commented on how to judge the R-factors.

A combination of techniques (including informed model building, computational model generation, Patterson or direct methods for SXRD data, electron microscopy, microcrystal diffraction and magic angle spinning NMR spectroscopy) has been proposed and summarised in the early work by McCusker for constructing a framework model.[27] Since then, much research has been devoted to building various other zeolite framework models using similar techniques.[28] To verify or confirm the constructed framework structure, high-resolution SXRD data is required to obtain more experimental observables for Rietveld refinement. More recently, there is significant progress in the complementary use of three-dimensional electron diffraction technique to PXRD for structure solution and phase identification; readers may refer to the review article by Xiaodong Zou, Wei Wan, et al. (2015) for more information.[29] Since the late 1980s, McCusker and co-workers have solved the crystal structures of some powder zeolite samples using the approaches mentioned above[30], e.g. the crystal structure of powder zeolite Sigma-2 sample has been determined without any prior structural information by combining Patterson

or direct methods with the Rietveld refinement of the SXRD data.[31] Two other supporting approaches have been later developed to facilitate building model frameworks and to study the effects associated with sample preferred orientation/textures.[32] Since then, many zeolite crystal structures have been determined by SXRD, such as ZSM-11 by Cox et al.[33] and ITQ-34 by Corma et al.[34] In 2009, the structure of mesoporous chiral ITQ-37 zeolite (see Figure 2) has been determined by a combination of SXRD and electron diffraction by the charge flipping algorithm by Sun et al.[35] Aside from typical aluminosilicate zeolites[36], there are two other commonly known classes of crystalline microporous inorganic solids that resemble similar structural properties of zeolites, namely aluminophosphates (AlPOs)[37] and silicoaluminophosphates (SAPOs).[38] These phosphate materials were developed by Flanigen and co-workers in Union Carbide Corporation (USA) and were published in 1982 for AlPOs and in 1984 for SAPOs. The crystal structures of these materials include novel structures, structures that are topologically related to zeolite, and structures that are topologically related between AlPOs and SAPOs[39]. In short, the direct determination of crystal structures does not always require single-crystal XRD measurements that require single-crystal samples (that are sometimes impossible to grow into sufficiently high quality). The rapid advances in synchrotron X-ray beam brilliance, diffraction instrumentation and high-quality detector allow the determination of crystal structure of powder within experimentally tolerable error.

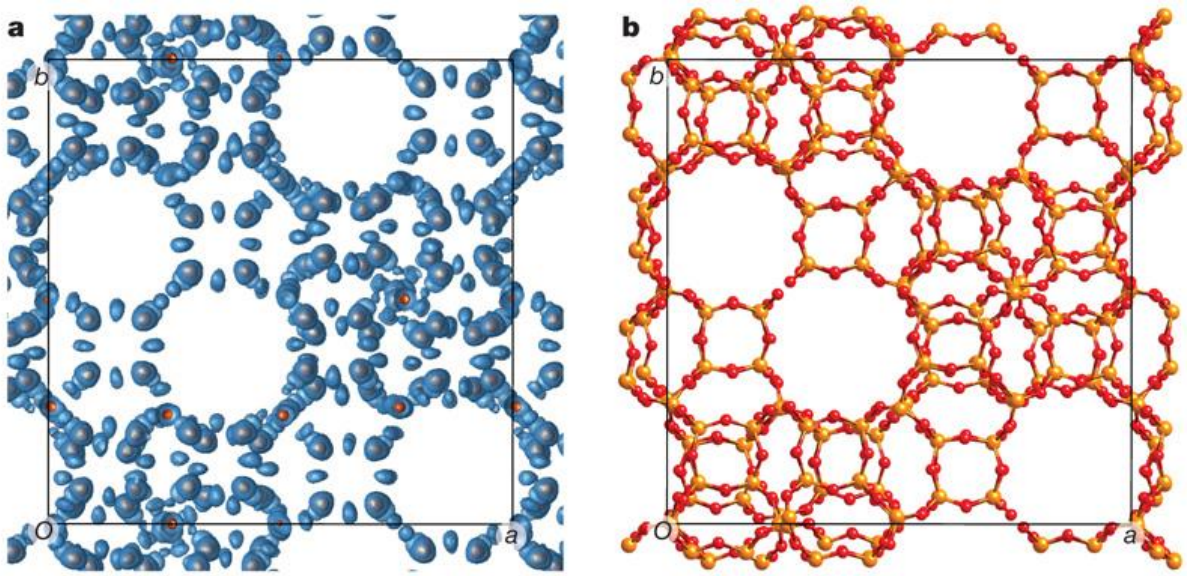

Figure 2. Zeolite ITQ-37 by Sun et al., with permission for reproduction[35], (**a**) the electron density map derived by the charge-flipping algorithm and (**b**) the obtained structure model, both are viewed along the *c*-axis.

For the interest of beginners for SXRD experiments, the remaining of this introduction entails some basics of PXRD, data acquisition and data modelling. PXRD and various microscopy techniques have generally been used to determine the topology of zeolites and some other crystallographic information. PXRD is well-established for structure refinements, particularly when sufficiently large single-crystals are not available. Typically, a high-precision diffractometer and a monochromatic X-ray beam, Cu or Mo K_α radiation is used in an angular dispersive instrument. Detailed descriptions of PXRD can be found in elementary textbooks by Dinnebier & Billinge (2008).[40] PXRD combined with Rietveld refinement (see below), especially when using powerful synchrotron X-ray beam, can reveal small details in the three-dimensional microporous structures of zeolites including the detailed atomic parameters: fractional atomic coordinates, SOF, and ADP. Although specialised, SXRD is also a well-established technique and provides higher resolution data in general (see below). The methodology is described in detail by Cockcroft & Fitch (2008)[18] and Wilmott (2011)[41].

PXRD has long been regarded as an indispensable crystallographic technique in studying the structure of zeolites. The most basic use of PXRD is the 'fingerprint' phase identification; different zeolites

produce different PXRD patterns (see Figure 3). As early as the 1970s, crystallographers have started to use the Rietveld method to solve and refine the atomic parameters of the framework atoms of zeolites.[22] In addition to the crystal structure, other crystallographic information could be obtained from PXRD by refinements, e.g. the topology, 'apparent' crystal size, strain or stress, extent of heteroatom substitution, crystallinity including lattice imperfections such as stacking faults, dislocation and atomic species disorder, etc.[5]

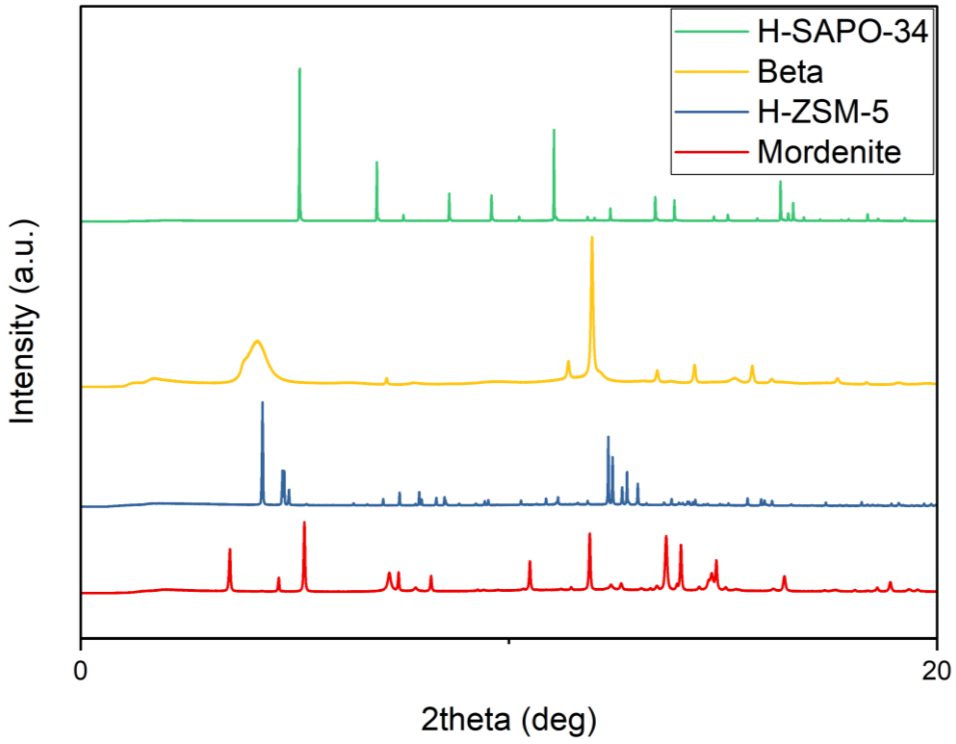

Figure 3. SXRD patterns collected on Beamline I11 in Diamond – 'fingerprint' phase identification. The wavelength was 0.825875(2) Å and the 2θ zero-point was -0.007547(3)°.

As mention, the diffraction technique originates from the discovery of William Lawrence Bragg and his father William Henry Bragg in 1912, that a crystalline material generates unique patterns of diffracted X-ray, distributed according to Bragg's law[42]. In short, diffraction occurs when Bragg's law is satisfied, where intense peaks of diffracted X-rays are detected at certain X-ray wavelengths and incident radiation angles (θ), which also applies to electron diffraction and neutron diffraction (ND). Bragg peaks are observed when the scattered X-ray beams constructively interfere (where n is an integer). Bragg's law can be described by the equation below:

$$2d\sin\theta = n\lambda$$

where d is the inter-planar distance,

θ is the scattering angle,

n is an integer, and

λ is the wavelength of the incident X-ray.

In principle, irradiated X-rays are scattered by the electrons surrounding an atom. At low 2θ angles, the scattering factor for an atom is nearly proportional to the number of electrons. Therefore, light atoms are weak X-ray scatterers, whereas heavy atoms are strong X-ray scatterers. In contrast, at high 2θ angles, the scattering factor decreases rapidly due to the partial interference of X-rays away from the incident angle of the beam. Thus, there is a general decrease over the Bragg peak intensity.

Indeed, both single-crystal XRD and PXRD can be used to study the structure of zeolites. When studying zeolite chemistry, PXRD is more commonly used due to its superiority in a vast number of particle sampling (true representation of bulk behaviour) when the specimen is subjected to non-ambient conditions or *in situ* environments. However, a major disadvantage of PXRD is the overlap of Bragg peaks. The use of high-resolution SXRD (to improve peak separation) has mitigated to some extent the issue. Later in 1977, a whole-pattern refinement method was developed by Hugo M. Rietveld, the Rietveld refinement. It can independently calculate these overlapping peaks, which allows a more accurate determination of the crystal structure.[43]

The most basic use of PXRD in zeolites is the structural identification and impurity determination. The first step to understand an unknown diffraction pattern is to 'index' the Bragg peaks as they can be assigned to their corresponding Miller *hkl* indices according to the space group symmetry of a structure. Herein, an investigator can extrapolate the lattice settings (i.e. cubic or monoclinic, etc.) and the space groups of the zeolite samples. After 'indexing' that reveals the lattice setting and space group of a zeolite sample, an investigator can then perform 'structure solution' to determine the crystallographic parameters, such as the lattice strain/stress, apparent crystalline size and lattice parameters. To solve the zeolite structure, different methods were reported in the past, such as the Pawley method, direct space method, Monte Carlo method, Patterson method, Le Bail method and multiple wavelengths phasing.[23, 44] For instance, the Le Bail method can reveal the crystallographic parameters. It uses a least-squares algorithm over the whole diffraction pattern, where the background, peak shape function parameters, and lattice parameters can be refined together (provided there are sufficient experimental observables). A significant advantage is the input of instrumental parameters is not compulsory, where an analytic peak shape function can be used instead. Since the Le Bail method is a whole-pattern refinement technique, even the overlapped peaks can be calculated during the refinement process.

The next procedure is 'structure refinement' that refines the atomic parameters of a crystal structure. The most commonly used structure refinement method is the Rietveld refinement. It is a whole-pattern fitting method using a non-linear least-squares procedure.[22] The non-linear least-squares procedure minimises the quantity based on the calculated and observed peak intensity, with applied weighting statistics. The three contributors of the Bragg peaks are sample lattice, diffraction optic effects, and instrumental effects. The Bragg peak intensity, I_{hkl}, is calculated as:

$$I_{hkl} = s\Sigma_{hkl} Lm_{hkl}|F_{hkl}|^2\varphi(2\theta_i-2\theta_{hkl})P_{hkl}A+I_{bi}$$

where s is the overall scale factor,

hkl represents the Miller plane indices,

L is the Lorentz-polarisation factor,

m_{hkl} is the multiplicity associated with the hkl plane,

F_{hkl} is the structure factor for the Bragg peak of the hkl plane,

$\varphi(2\theta_i-2\theta_{hkl})$ is the profile function, where $2\theta_i$ is corrected for 2θ zero error,

P_{hkl} is the preferred orientation function,

A is the absorption factor, and

I_{bi} is the background scattering intensity at the i^{th} step.

The structure factor (F_{hkl}) of a unit cell describes the Bragg peak of the hkl plane which contains the structural information:

$$F_{hkl} = \Sigma f_j g_j[exp-2\pi i(hx_j+ky_j+lz_j)]exp(-B_j sin2\theta/\lambda^2)$$

where f_j is the scattering factor of the atom j,

g_j is the site occupancy factor (SOF),

x_j, y_j, and z_j are the fractional atomic coordinates of the atom j, and

B_j is a measure of the root-mean-square amplitude of atomic displacement.

Note that some planes overlap but they possess different structure factors. For example, in a cubic lattice, the 511 and 333 reflections possess identical lattice *d*-spacing. As the Rietveld refinement is a whole-pattern fitting technique that involves all the structural parameters, when the peak intensity is calculated, the overlapped Bragg peaks can be resolved. The Rietveld refinement allows simultaneous refinements (and adjustments) of structural parameters, e.g. peak profile, unit cell, background, etc. Thus, the least-square algorithm allows an improvement of the structural model, which is continuously fed back during the refinement.[22] By using the derivatives of the parameters in the least-squares minimisation equation with respect to zero, a set of non-linear equations can be obtained. By solving these derived non-linear equations using an $n \times n$ matrix, the solution is refined relative to the starting parameters, until the solution ultimately converges.[22] Hence, the least-square refinement procedure ensures the global minimum of the parameters is met.

As the incidental effects due to the very close lattice parameters that may lead to severe peak overlap, a high-quality and well-aligned instrument with high-resolution data is necessary for the Rietveld refinement work. Owing to the advancement of the synchrotron X-ray facilities around the globe, the PXRD pattern using synchrotron X-ray radiation can achieve much higher peak resolution due to better diffraction instrumentation. High-resolution SXRD data is critical to detect any subtle change in the sample, where high-resolution here refers to (i) high angular resolution and (ii) high accuracy and reliability of the intensity of the Bragg peaks. In a well-established high-resolution SXRD beamline (such as Beamline I11 in Diamond and Beamline ID22 in ESRF), a typical set-up is very often in place for ambient measurements. The energy (wavelength) of the X-ray beam and other instrumental calibrations (such as 2θ zero-point and detector offset) are calibrated against high-quality Si or CeO_2 standard. The energy of the synchrotron X-ray beam varies between samples, which normally ranges between 15-25 keV. The higher is the energy, the lower is the flux density (photons s^{-1} per 0.01% bandpass), but the lower is the X-ray absorption.[45] Briefly, the energy of the synchrotron X-ray beam should be chosen based on the following criteria: (i) to reduce Bragg peak overlap, and (ii) low X-ray absorption of the sample (which can be computed; readers may refer to this website for reference: http://11bm.xray.aps.anl.gov/absorb/absorb.php).[46] Fine powder samples should be loaded in a thin borosilicate or quartz capillary (typically with a diameter of 0.5 mm); fast sample spinning is essential to bring more crystallites into the Bragg diffraction condition. There are two types of detectors in some beamlines, namely multi-analyser crystals (MAC) detector and MYTHEN position sensitive detector (PSD, Dectris).[46] If time is available, it is advised to first use the MAC detector to collect a set high-resolution data, and then employ the PSD for dynamic and kinetic study. A MAC detector scan typically takes half to an hour for good averaging statistics, whereas a PSD scan can take down to several seconds. Some beamlines, such as Beamline I11 in Diamond, Beamline ID22 in ESRF and many others, already have specifically developed cells for *in situ* or *operando* SXRD measurements. In the *in situ* studies described in Sections 3 and 4 by Tsang group, a both-way open-ended capillary reactor cell (which can withstand temperature between 80 K – 1273 K, and pressure up to 100 bar) was used for catalytic reactions under SXRD in a controllable manner (see Figure 4). The sample (*ca.* 0.5 mg) was sandwiched between two pieces of quartz wool in the capillary to prevent sample dislocation. One end of the capillary was connected to a gas inlet, while the other end was connected to a quadrupole mass spectrometer (MS) that analysed the gas composition on-line with simultaneous SXRD data collection. Complete blockage of the capillary (no gas flow) can be common, which can be detected by an external gas flow meter. This is particularly common if the samples contain very fine powder. A sieve fraction can be used to control the range of the powder particles to avoid back pressure build-up. The space velocity should be adjusted based on the actual mass of the sample loaded in the capillary. In addition, the dead volume between the MS and the reactor cell should be recorded and kept minimal. It is technically challenging to achieve spinning of the capillary. A constant capillary rocking generated by the sample stage holder can thus be employed to reduce the constant X-ray beam exposure to any preferred orientations of the individual grains in the powder sample during measurements.

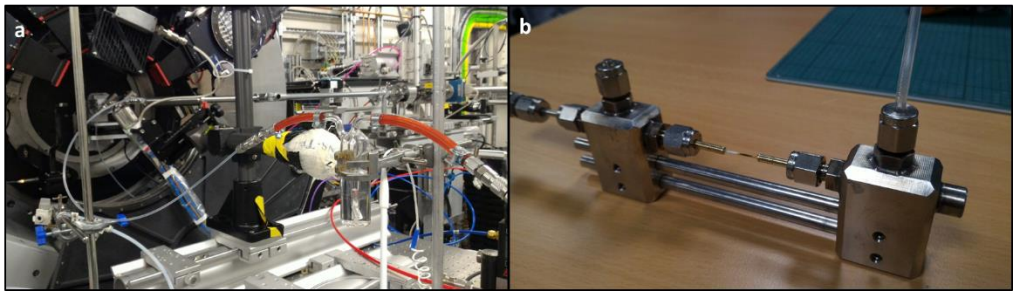

Figure 4. On-line SXRD-MS set-up on Beamline I11 in Diamond. (**a**) A high-pressure gas cell with one end of the both-way open-ended capillary (diameter of 0.7 mm) is connected to inlet reaction substrate vapour, with the other end connected to the mass spectrometer for on-line gas analysis. To conduct high-temperature experiments, a hot-air blower (RT – 1000 °C) is also in place. (**b**) The high-pressure gas-cell with stainless-steel support for capillary alignment.

These following two paragraphs cover some strategies for data analysis and modelling. At present, various commercial and open-source programmes are commonly used for structure solution and Rietveld refinement, including *TOPAS* (Bruker) developed by Alan Coelho[47] and *GSAS-II* developed by Toby and Von Dreele[48]. Over the studies described here, the determination of guest species in the zeolite framework is primarily concerned, which will therefore be highlighted in these paragraphs. In general, the crystal structures of most zeolites of high application values/interests have already been solved, such as H-ZSM-5, mordenite and H-Y. It is essential to first determine the quality of the SXRD pattern by checking the presence of any impurity peaks. This can be achieved by Pawley/Le Bail refinement, where the basic X-ray parameters, space group and approximate lattice parameters of the sample should be prior known (from literature). Basic refinement parameters include the Chebyshev polynomial background coefficients and scale factors. A mathematical peak shape function is commonly used to model the effects caused by the instruments and sample.[49] A refined set of lattice parameters can then be used for the subsequent Rietveld refinement. It is warned that the Rietveld refinement process may sometimes fail due to inaccurate lattice parameters.

To start a Rietveld refinement, the fractional atomic coordinates of the structure are advised to be adopted from a respected publication. In principle, upon organic molecule adsorption, the positions of the framework atoms may change slightly. Therefore, before the refinement including the guest molecules, the framework atoms can be first refined to avoid a miscalculation of the structure. As the guest organic molecules do not contain any heavy atoms, it is reasonable to assume the guest molecules only minimally contribute to the low 2θ angle Bragg peaks. In work by Tsang group, the fractional atomic coordinates of the framework Si and O atoms were first independently refined over the high 2θ range.[50] Over the whole fitting range, the Fourier analysis (electron contrast map) was then used to identify the positions with the highest remaining electron density in the framework. A Monte Carlo-based simulated annealing technique was followed to locate the positions of the guest molecules in the zeolites. The guest molecules can be described by rigid body Z-matrices. For the first attempts determining the number of the guest molecule sites before collecting their locations by the simulated annealing method, the fractional atomic coordinates of the framework atoms should be fixed. At last, all the relevant parameters should be refined by simulated annealing repeatedly to ensure the global minimum has been reached.

Even though SXRD has a much higher angular resolution than PXRD, the intrinsic limitations of powder diffraction should still be noted. A much greater number of experimental observables is therefore required to ensure an accurate and reliable refinement (by the Rietveld refinement method) of SXRD data. A measure has often been used by crystallographers to limit the total number of refinement parameters, i.e. the application of refinement constraints. For instance, in work by Fitch et al.[51], as the isotropic ADP (u_{iso}, note that $u = B / 8\pi^2$) and site occupancy factors (SOF) are strongly correlated, the u_{iso} values of the adsorbed molecules were set (constrained) at 0.08 Å^2, and the SOF of pyridine was set (constrained) at 1.5 molecules per supercage. In the work mentioned above by Wragg et al., the u_{iso} values of the adsorbed methanol species were fixed, with those of the C and O atoms at 0.038 Å^2 and

the H atoms at 1.2 times those of the C/O atoms (at 0.0456 Å^2). In the studies by Lo and co-workers[50, 52–54], the u_{iso} values of the framework O atoms were refined but were set at two times that of the framework T (T = Al or Si) atoms. In a typical study of H-ZSM-5 by Lo and co-workers, over the Rietveld refinement 2θ range of 3-55°, there are about 4200 experimental observables (*hkl* reflections) with a much lower number (below 180) of refinement parameters. This allows accurate and reliable Rietveld refinement works for the determination of bond/interatomic distances at an atomistic level.

2. Adsorbate-framework structures in zeolites

Owing to a higher X-ray beam brilliance and more accurate diffraction facilities in determining diffraction peak width and height by synchrotron X-rays allow the detection of organic-based adsorbate molecules due to a slight but significant alteration in the scattering parameters of the framework atoms in close proximity.[50] Efforts by McCusker, Fitch and co-workers should be acknowledged since the late 1980s who have probed the presence of adsorbate molecules in zeolites.[31, 51] Recently, the interatomic distances between the adsorbed methanol molecules and the framework SAPO-34 atoms have been measured by Wragg et al. (see Figure 5).[55] Even without synchrotron X-rays, a handful of works using conventional laboratory PXRD instrument have successfully detected adsorbed pyridine[56] and benzene[57] in H-ZSM-5, as well as methyl tertiary butyl ether and toluene in mordenite but with a higher degree of errors.[58] Readers may also refer to the review chapter in Structure and Bonding by Smeets and McCusker (2017)[59] for more examples for probing the organic structure-directing agents in various zeolite frameworks.

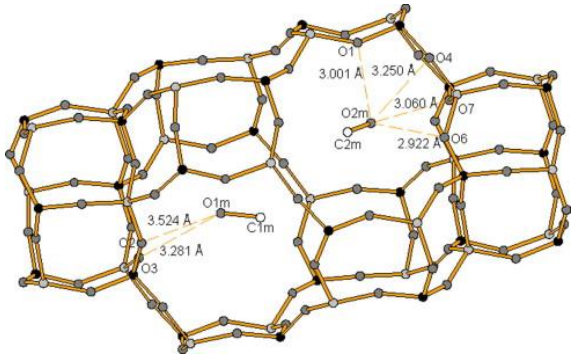

Figure 5. Location of the adsorbed methanol molecules in SAPO-34 with oxygen to framework contacts shown as dotted lines labelled with distances, with permission for reproduction.[55]

One of the most important contributions of this technique is to guide the rational design of new zeolite systems. This may involve the structural elucidation of the interactions between small organic molecule substrates with the active sites, such as BAS and LAS, in the zeolite framework. Thus, a reliable experimental method is necessary to reveal the atomic arrangement of the organic adsorbates with respect to the internal active sites. With more relevance to zeolite catalysis studies, SXRD can be applied to investigate the structural properties of the zeolite frameworks. Note that the H species of the BAS cannot be directly visualised by any X-ray technique as X-rays only 'see' electron clouds. A simple way has been used by Pinar et al. and Lo et al., which gauges the location of the BAS (hence the Al site) by examining the interatomic distances and angles between the framework O atoms and the lone-pair electrons donor of the basic probe molecules.[50, 60] Pinar et al. have shown the location of Al sites in ferrierite zeolite can be controlled and consequently probed using organic structure-directing agents.[60] Through the study of the locations of three adsorbed basic probe molecules (namely, pyridine, ammonia, and methanol) in H-ZSM-5 zeolite (see Figure 6) by Lo et al., all the most strongly adsorbed species (determined by TGA) are found to locate in the sinusoidal-straight cross-channel region of the H-ZSM-5 framework. This agrees with the earlier postulations from spectroscopic and modelling characterisations that the BAS are likely to be located in the cross-channel region in H-ZSM-5.[61] The three basic probe molecules form a near bidentate interaction with the framework. The Brønsted acid-base interactions have been analysed in terms of interatomic distances and angles.[50] In the specific commercial H-ZSM-5 sample, the BAS has been inferred at the framework O18 position, with the substituted Al site at the framework T6 position.[50, 52] This offers a reliable tool in determining the adsorbate-framework interaction in zeolites. The work suggests the intrinsic acidity is not the only parameter that influences molecular adsorption, but the stereospecificity of the zeolite framework and adsorbed molecules should also be considered. It is envisaged that more critical information can be obtained for the design and engineering of zeolite catalysts, such as the spatial arrangement and concentration of the active BAS and LAS.

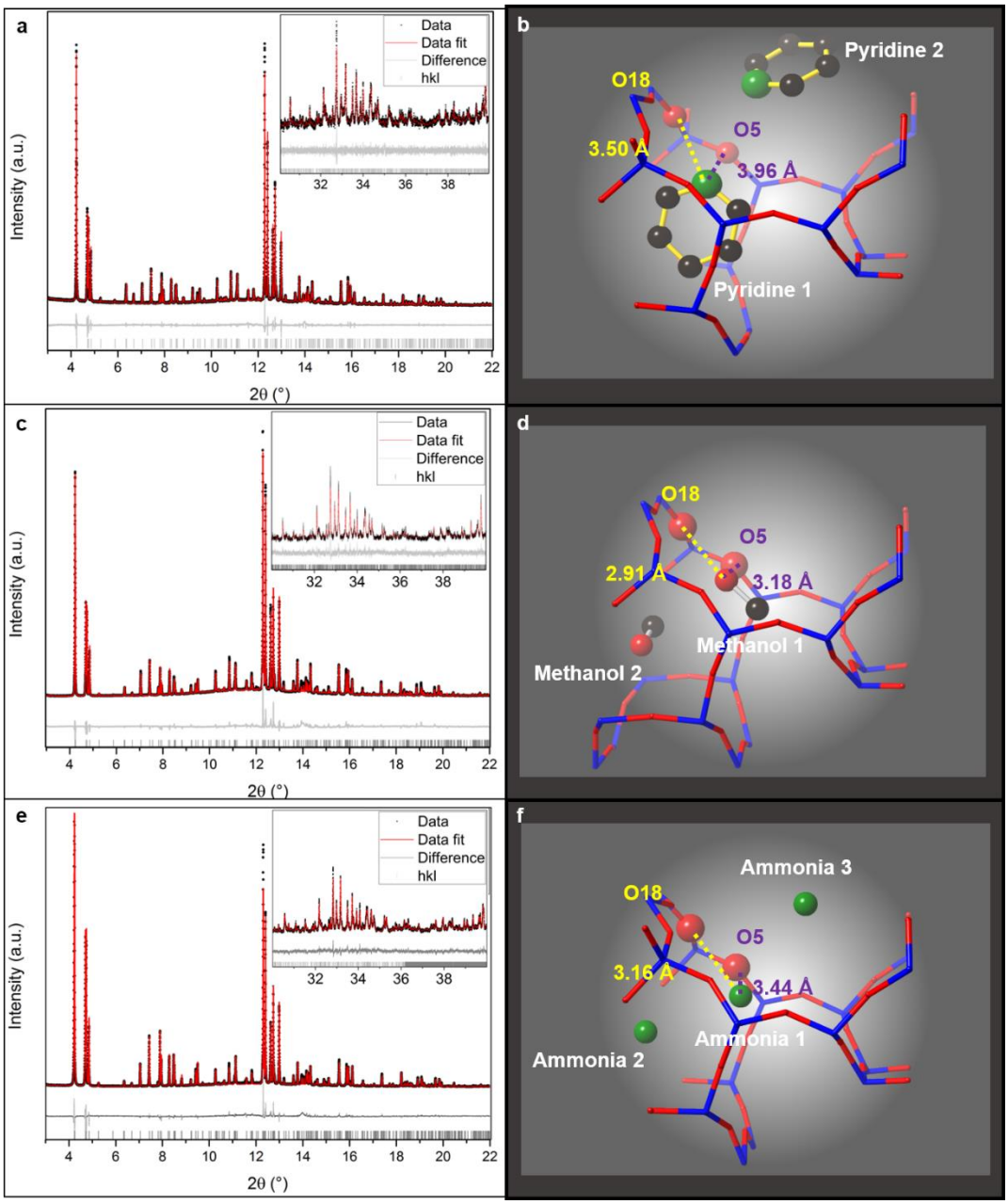

Figure 6. SXRD patterns and Rietveld refinement profiles of H-ZSM-5 pre-adsorbed with (**a**) pyridine, (**c**) methanol, (**e**) ammonia at 25 °C, and the corresponding crystal models were constructed and displayed in (**b**) pyridine, (**d**) methanol, and (**f**) ammonia with the unit cell from [010] direction (straight channel view), with permission for reproduction. Ball-and-stick model: blue = Si/Al, red = O, green = N, and black = C. H atoms are omitted for clarity.[50]

Tsang group have also recently reported a novel catalytic biomass conversion over H-Y zeolite in a 'one-pot' synthesis process via the Diels-Alder reaction mechanism. It replaces traditionally used gaseous ethylene by liquid ethanol for the conversion of 2,5-dimethylfuran (DMF) into various useful aromatic products.[53] The rate of reaction has been reported about three times faster when ethanol is used as the reaction substrate. To investigate this promotion effect, Tsang et al. have combined SXRD with density functional theory (DFT) calculation. Both techniques have shown that ethanol is preferentially protonated by the BAS of the framework (see Figure 7). This preferential protonation has been proposed to lead to a higher local concentration of ethylene around the BAS, via acid-catalysed ethanol dehydration. It eventually increases the rate of Diels-Alder (DA) reaction between furan and the newly formed ethene. With the subsequent dehydration, aromatic products can be formed. H-Y zeolite shows

superior activity and selectivity for DA and dehydration reactions to that of H-ZSM-5 due to the larger internal porous cavity. Such an example illustrates that SXRD – in combination with other analytical tools – can also be used to provide mechanistic information over catalytic reactions in zeolite materials with spatial characteristics.

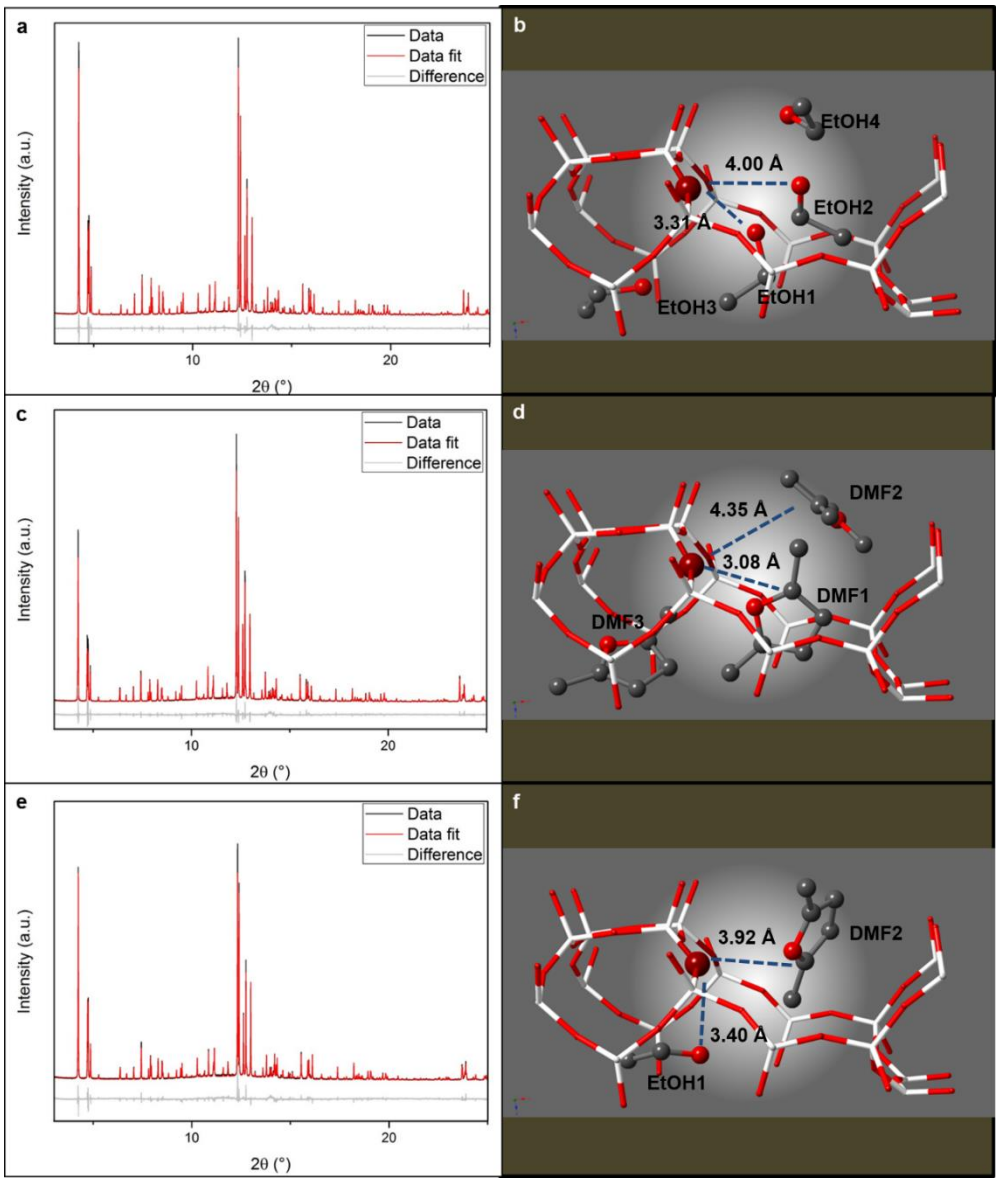

Figure 7. SXRD patterns and Rietveld refinement profiles of H-ZSM-5 pre-adsorbed with (**a**) ethanol (EtOH), (**c**) 2,5-dimethylfuran (DMF), and (**e**) EtOH/DMF at 25 °C, and the corresponding crystal structures viewing from the [010] direction are displayed; (**b**) EtOH, (**d**) DMF, (**f**) EtOH/DMF, with permission for reproduction.[53] Ball-and-stick model: white = Si/Al, red = O, and black = C. H atoms are omitted for clarity.

The above work by Lo et al. offers a reliable SXRD methodology in determining the substituted Al sites within the zeolite framework, which is believed to be transferable to other zeolites. In fact, the hydrogen atoms (or deuterium) associated with the BAS inferring the substitution position of Al in zeolites can be accurately detected using powder neutron diffraction (ND).[62, 63] Early ND work has also demonstrated its capability to detect organic adsorbed species in zeolites. Unlike X-rays, neutrons are scattered by nuclei (a point) rather than from electrons (diffused). The variation of the neutron scattering factors (a.k.a. scattering lengths) behaves differently from that of the X-ray analogues. The presence of positive and negative scattering factors makes ND a handy tool in identifying different species from the Fourier contrast maps. Previous crystallographic attempts have been made to observe the presence of

organic molecules in various zeolites. Notably by Taylor, Czjzek, Fitch and Vogt, different large organic molecules (e.g. aniline, deuterated benzene and pyridine) in various zeolites using ND or in combination with SXRD have been studied since the late 1980s.[63–65] More recently, Long et al. found the CO_2 adsorption sites in Ca-A zeolite (see Figure 8).[66] However, while ND is sensitive to light elements, it is difficult to study the *in situ* chemistry in zeolites using ND on its own. In general, when compared with SXRD, ND requires significantly longer data collection time, larger sample sizes due to lower neutron flux and smaller beam cross-section. The complex ND instrumentation also leads to limited availability and difficulties in carrying out *in situ* or *operando* catalysis experiments. Thus, although the combination of SXRD and ND can offer valuable and complementary diffraction data if both techniques can be made available, it may not always be necessary to be the case in dealing with practical zeolite study.

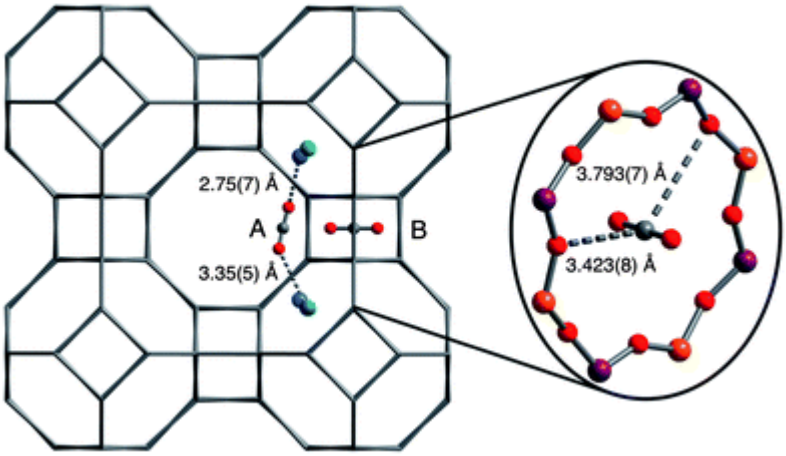

Figure 8. Structures associated with CO_2 adsorption at sites A and B in zeolite Ca-A, as determined from neutron powder diffraction at 10 K. Grey, red, blue, green, orange, and purple spheres represent C, O, Na, Ca, Al, and Si atoms, respectively. Note that cations in the 6-ring sites are disordered such that a given CO_2 at site A may interact with two Na^+ atoms, two Ca^{2+} atoms, or one Na^+ atom and one Ca^{2+} atom (as depicted). A molecule of CO_2 adsorbed in an 8-ring (site B) is shown at the right, Reproduced from Ref. 66 with permission from The Royal Society of Chemistry.[66]

In brief, SXRD in combination with other analytical techniques has proved to be a practical and powerful toolkit for the study the adsorbate-framework relationships. Not only the adsorption interactions can be probed in terms of interatomic/bond distances and angles, but some critical mechanistic information of various zeolite catalytic reactions can also be inferred.

3. Gas separation and gas storage

Due to the well-defined molecular-sized pores, high porosity, high thermal and chemical stability and intrinsic acidities, zeolites are widely used for gas separation and are potential candidates for gas storage. Their gas separation properties have been summarised in the review article by Kosinov et al.: size exclusion, diffusion selectivity and adsorption strengths.[67] SXRD can offer critical information to investigate the gas separation properties, such as the channel dimension with respect to the size of the gas molecules, the adsorption strength between different species, the location, interaction and total quantity of gaseous guest molecules stored in the porous zeolite structures, which can allow rational design of solid adsorbents.

A notable example that applies SXRD in the study of 'discriminative' gas separation in zeolites is by Webley et al.[68] The work has revealed how the change in the occupation of the Cs^+ 'doorway' site can greatly affect the discriminative gas separation performance. High selectivity in the separation of important industrial gas mixtures such as CO_2/CH_4 and counterintuitive size-inverse sieving of CO/N_2 by a Cs^+-containing chabazite zeolite is designed (see Figure 9). Furthermore, Tsang group have recently investigated the SAPO-34 zeolite during methanol conversion to hydrocarbons (MTH) at high temperature using SXRD. The adsorption capability of butene of large dynamic size has been significantly reduced, whereas those of ethene and propene of smaller sizes have not changed during the initiation period of the catalytic reaction. This is shown to relate to the *in situ* formation of adsorbed surface methoxy species at the window opening of SAPO-34, which reduces the dynamic size of the window opening (see Figure 10). As the kinetic diameter of butene is akin the dimension of the window, the subtle change in window size has an observable effect on the production of butene. Therefore, the molecular sieving properties of SAPO-34 can be dynamically modified in favour of small size olefins production [unpublished work].

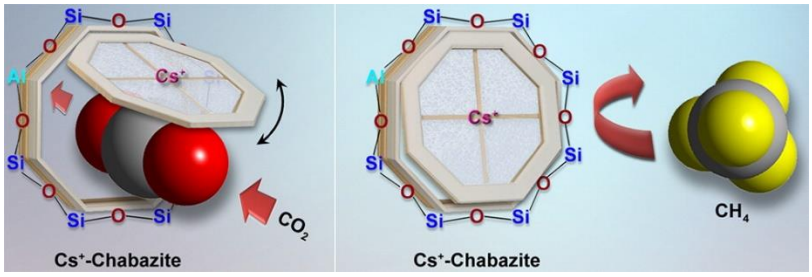

Figure 9. A Cs^+ 'trapdoor' in Cs^+-chabazite that selectivity separate important industrial gas mixtures such as CO_2/CH_4, with permission for reproduction.[68]

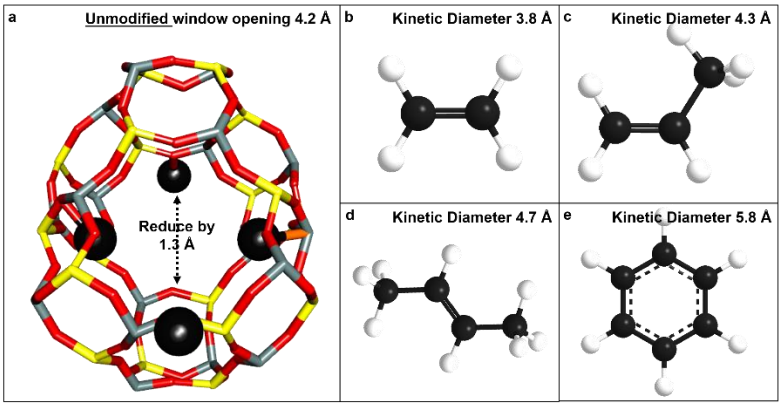

Figure 10. (**a**) Rietveld derived crystal structure of framework atoms; the pore opening can be reduced by as much as 1.3 Å in one dimension (estimated by the CrystalMaker software). Grey = Si/Al, yellow = P, red = O, and black = C. No hydrogens are plotted for clarity. (**b**) – (**e**) Displays of ethene, propene, trans-2-butene, and benzene, with their corresponding estimated kinetic diameters [unpublished work].

For gas storage in zeolites, the latest research has focused on how to effectively store functional gases that are mostly related to energy supply and storage. Not only the atomic information of gas molecules with respect to the framework can be studied, but the kinetic information that may facilitate the design and engineering of zeolites in gas storage can also be revealed. Although hydrogen cannot be detected by X-ray techniques, when hydrogen storage was proposed as a viable alternative for mobile energy provision in the 1990s, SXRD has been employed to study zeolites extensively carried out. It is because zeolites are promising candidates with high potential for storing hydrogen due to strong anticipated wall effects. The hydrogen storage performance in various zeolites and microporous carbon synthesised by a zeolite templating method has been evaluated.[69–72]

Another great example is ammonia storage in zeolites. Aside from the extensive use of ammonia as a fertiliser precursor chemical, ammonia is also a possible carbon-free fuel candidate. This offers an exciting potential for ammonia to be used in energy storage with higher energy density than liquid hydrogen[73], where ammonia is stored due to the BAS and LAS in zeolites. At the ammonia release stage, some ammonia may be released under low energy input condition, but some may require high temperature without a clear rationale. The work by Ye et al. presented the kinetic information of ammonia desorption from H-ZSM-5 zeolite by combining *in situ* SXRD and TGA. It is found that there are different strengths of ammonia adsorption sites within in the framework (see Figure 11). It has been postulated that the ammonia molecules are interconnected via their hydrogen moieties by forming a hydrogen bonding network. Three desorption steps were reported, with the apparent desorption energies of 7, 21 and 113 kJ mol^{-1}. These interactions can be rationalised in the forms of physisorption, intermolecular hydrogen bonding, and Brønsted acid-base adducts, respectively. This work reveals why multiple release steps are frequently observed in many ammonia storage materials. By changing the acid strength and spatial arrangement of the acid sites, it is envisaged that the ammonia storage properties can be well-engineered.[52]

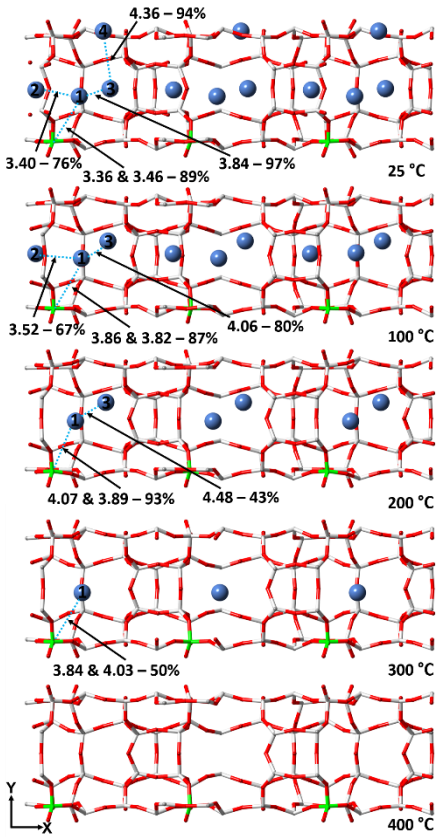

Figure 11. Rietveld derived crystal structures of temperature programmed *in situ* SXRD measurements of H-ZSM-5 pre-adsorbed with ammonia. The numerical values represent the interatomic distances, whereas the percentage values correspond to the SOF values of the corresponding sites. Ball-and-stick model: blue = N, red = O, white = Si, and light green = Al, with permission for reproduction.[52]

4. Extra-framework metal species

The inherent zeolitic microporosity and periodicity provide a perfect and well-defined environment for cationic metal species (such as Na^+ and Zn^{2+}) to replace the BAS protons via ion-exchange. They then interact with the negatively charged framework via electrostatic interaction. Some metal species may further anchor onto the zeolite framework by thermal dehydration.[74, 75] Many catalytic reactions are found facilitated by ion-exchanged zeolites[12, 76], e.g. the selective catalytic reduction of nitrous oxides (NO_x) over Ni- and Pd-ZSM-5, and Cu-SSZ-13[77–79], the production of aromatic products from methanol feedstock Ag-, Zn-, and Ga-ZSM-5[80], the para-selective halogenation of aromatics over various zeolites exchanged K^+ [81]. However, the metal anchoring process and the role of transition metal ions to substrate molecules are still unclear. SXRD can continue to shed light on the catalytic activity-structure relationships. Previous research has determined the locations of these metal species, such as Li, Na, K, Rb, Cu, and Tl in H-ZSM-5 by Mentzen and co-workers, which allows the rationalisation of active sites for specific catalysis.[75, 82] Upon a dehydration treatment of Cu-ZSM-5, new Cu sites locate very close to the zeolite framework. In light of the SXRD work, Mentzen et al. have postulated that these new metal sites might play an essential role in catalysis, as molecules can effectively diffuse through the channel void to gain access to the metal sites (see Figure 12)[75]. In addition to the traditional ion-exchange approach, grafted organometallic precursors have been employed to synthesise specific single-site organometallic species within the zeolite framework. Notable examples include the work of Hensen, Long and co-workers in exchanging $Ga(CH_3)_3$ with H-ZSM-5[83] and ferrocene with H-Y[84], respectively. Readers may refer to the review article by Frising and Leflaive[85] and van Santen[86] for more information about the extra-framework metal LAS, as well as the previous extensive work by Smith (1971)[87] by Mortier (1982)[88].

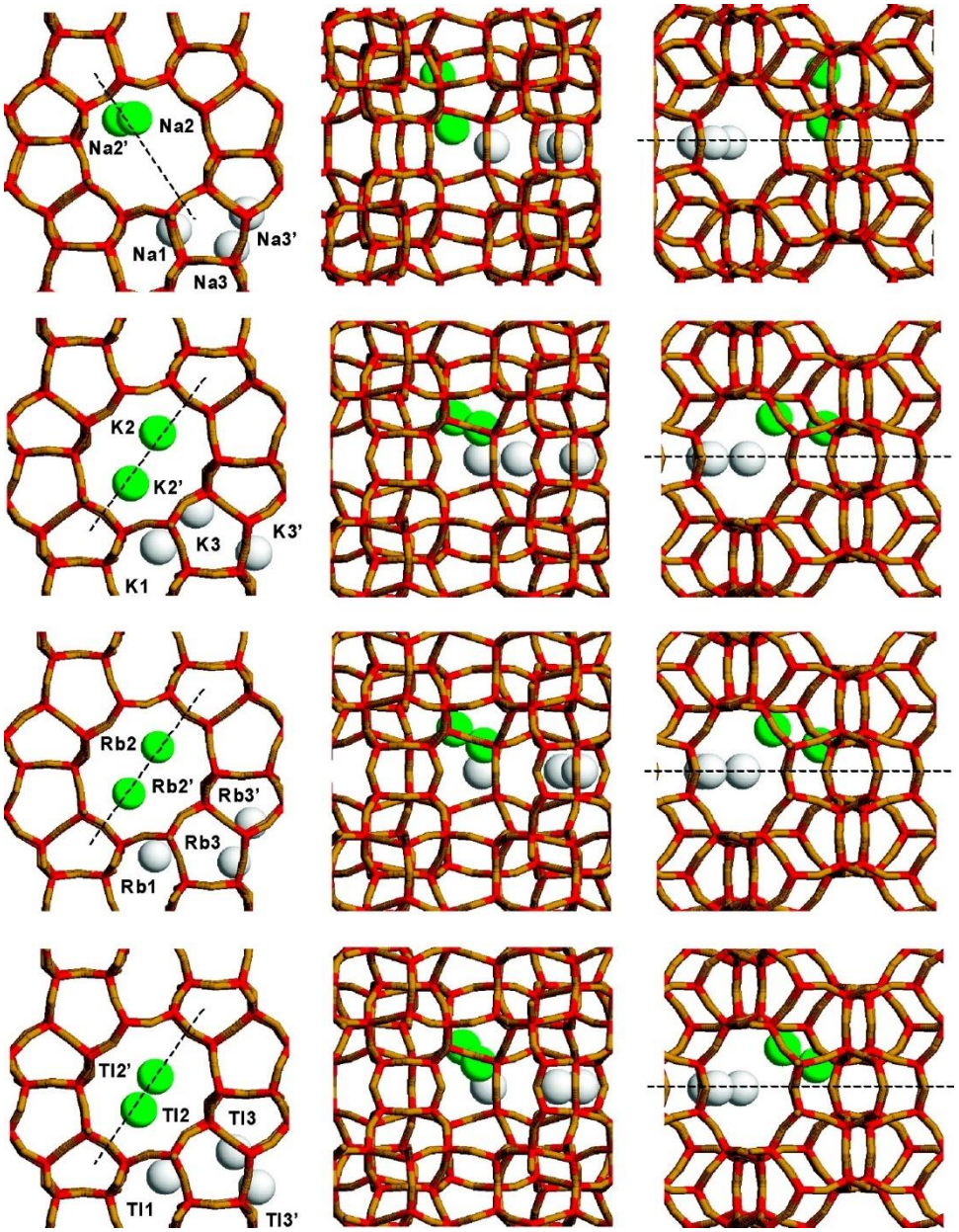

Figure 12. Comparison of the crystal structure of the Na-, K-, Rb-, and Tl[I]-exchanged **MFI**-type phases. The white spheres correspond to the cations located on the mirror plane (space group*: Pnma*), and the green spheres correspond to cations in or close to the straight channel sections. The left, middle, and right columns correspond to the views down the y-axis (straight channel), z-axis, and x-axis (zigzag channel) directions, respectively, with permission for reproduction.[82]

Extra-framework Al (EFAl) is very important in zeolite chemistry. It exhibits strong Lewis acidity, and can also enhance Brønsted acidity in zeolites.[89] In the preparation of USY (ultra-stable Y) zeolite from Y zeolite, mild-steaming treatment is commonly used to improve its hydrothermal stability.[90–92] During the steaming treatment, part of the framework Al were found leached into the extra-framework positions.[93] Previous attempts have been made to study the chemistry of the EFAl species using various spectroscopic techniques.[94] However, no spatial relationship of EFAl with the enhanced Brønsted acidity can be correlated. The EFAl positions in dealuminated NH_4−Y zeolite have been revealed for the first time by SXRD by van Bokhoven et al. (see Figure 13).[95] However, their crystallographic relationship between the Brønsted acidity and the neighbouring EFAl had still been unclear. Until recently, by employing SXRD in combination with basic probe pyridine, a 4-coordinate EFAl has been identified in the sodalite cage (see Figure 14), which directly polarises the adjacent framework O4 position of BAS, enhancing the strength of the BAS at this framework position.[96]

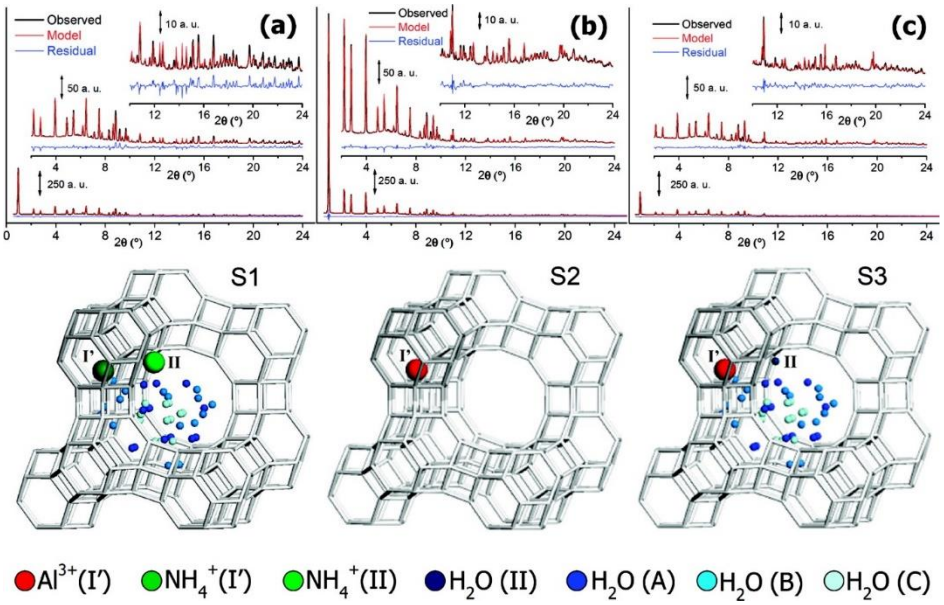

Figure 13. Refinements (top) and relative models (bottom) for the SXRD data, collected at various temperatures: 300 K, S1 (**a**); 873 K, S2 (**b**); 300 K, S3 (**c**). Top: Observed (black), calculated (red), and residual (blue) profiles. The zooms highlight the 2−24° and 10−24° 2θ regions to illustrate the quality of the data and the refinement. Bottom: Sticks representation of the Y zeolite framework showing one supercage and several sodalite cages together with the refined extra-framework (I′, II) and water (A, B, and C) sites, with permission for reproduction.[95]

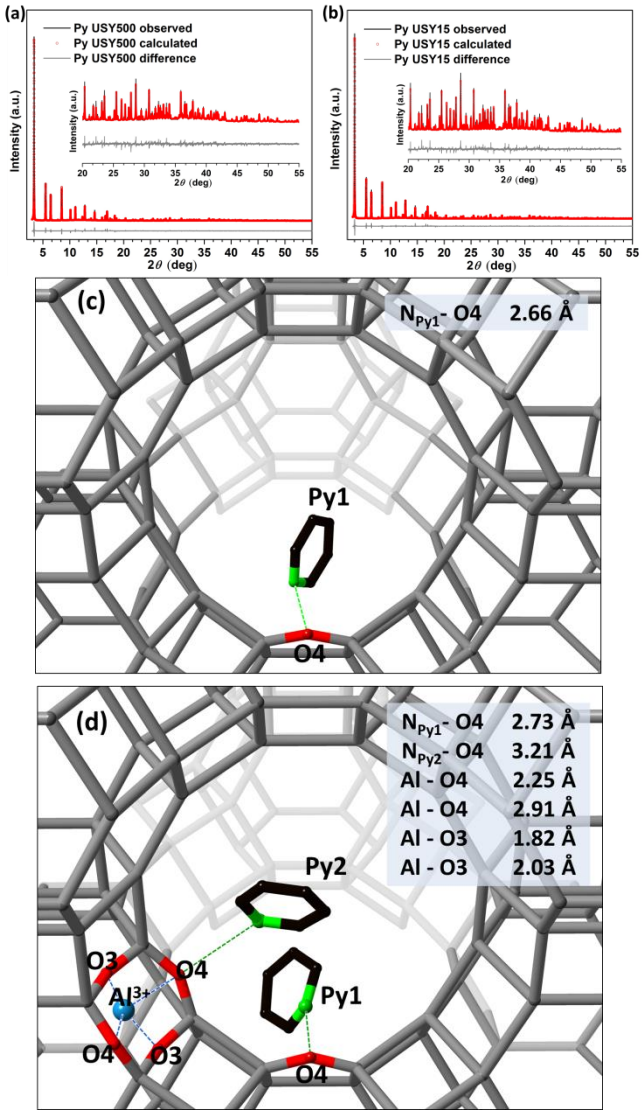

Figure 14. Rietveld refinement profiles of (**a**) USY500 and (**b**) USY15 with pre-adsorbed pyridine; (**c**, **d**) the corresponding derived crystal structures are presented, with permission for reproduction.[96]

Recently, extended X-ray fine absorption structure (EXAFS) has been combined with SXRD to determine the structures of various metal ion-exchanged zeolites. Whereas SXRD can be used to derive the bond distance and coordination environment from the metal site (via Rietveld refinement), EXAFS can also obtain these structural information directly. The data generated from these two techniques if agreeable can be used to improve the reliability of structural elucidation. Although EXAFS gives bond distances of metal ions that may not always reconcile with those derived from SXRD due to inherently different underlying principles, coordination environments and associated errors, the use of EXAFS data as a restraint in SXRD refinement can be especially useful when the number of occupied sites is small. This point has been shown by Beale et al. who combined the *in situ* SXRD and EXAFS to comprehensively study the local coordination geometry, redox functionality and precise location of the active isolated Cu site in Cu-SSZ-13 even at low metal concentration. They also extended their investigation to the structural properties with respect to the NH_3-selective catalytic reduction reaction.[79, 97] Further structure-activity investigation has been performed using similar techniques.[78]

Tsang group have combined SXRD, EXAFS and ssNMR to elucidate the structure of the active site in Zn-ZSM-5 zeolite catalyst and its interaction with organic substrate species. The atomic structure and geometry of the Zn^{2+} active centre and the neighbouring BAS in Zn-ZSM-5 have been undisputedly

determined. The synergy effect between the anchored Zn^{2+} site with the BAS is demonstrated to catalyse a novel one-step conversion of biomass-derived gamma-valerolactone (GVL) into aromatic products at high yield under aqueous condition. It is because the anchored Zn^{2+} in H-ZSM-5 (onto the zeolite framework) contains a terminal 'Zn-OH' group, which induces nucleophilic attack to the carbonyl of GVL for ring opening. The adsorption structure of GVL on the 'Zn-OH' site in Zn-ZSM-5 has also been for the first time demonstrated (see Figure 15). Such structure and mechanism for the nucleophilic attack of the active 'Zn-OH' site are comparable to that of the reported Zn-containing T199A-CA II enzyme in the biological system.[54]

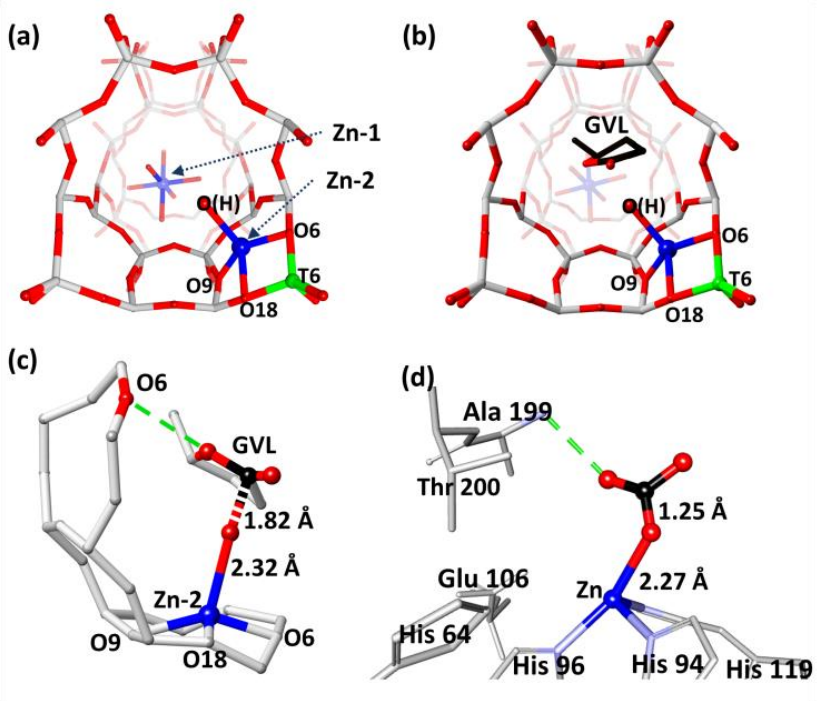

Figure 15. The refined structures of Zn/ZSM-5 catalyst derived from SXRD and refinements. (**a**) Zn/ZSM-5; (**b**) gamma-valerolactone (GVL) adsorbed on Zn/ZSM-5; (**c**) A close-up view of Zn-2-OH interacting with the carbonyl of GVL; (**d**) A published crystal structure showing a complex intermediate of Zn-OH of T199A-CA II enzyme with adsorbed CO_2 for comparison (PDB: 1CAM) with permission for reproduction.[54] Ball-and-stick model: O = red, Si = grey, Al = green, Zn = blue, and C = black.

5. *In situ*/*Operando* SXRD experiments for catalysis chemistry

An *in situ/operando* SXRD experiment can offer additional kinetic and dynamic information on how a material works in an applied external environment. It can be temperature programmed, time-resolved, with loaded gas, etc. In most *in situ* SXRD works, the data were collected using PSD (such as imaging plate, line detector, and area detector) instead of point MAC detectors, as this can reduce the data collection time down to the order of few seconds. An explicitly designed *in situ* set-up is necessary; a capillary gas-cell that can withstand high temperature and pressure SXRD experiment was designed and reported in the early work by Norby.[98] In fact, the ability to perform *in situ* experiment benefits from the significant improvement in synchrotron X-ray beam brilliance. A higher brilliance X-ray beam allows faster data collection. Before this generation of synchrotron X-ray facilities, a typical SXRD pattern would take hours for data collection. It makes *in situ* or *operando* catalysis study rather impractical. Further improvements in synchrotron X-ray beam intensity, reduced beam cross-section, detector sensitivity and reduced acquisition time would be anticipated for a wider application of this technique to study the dynamic behaviour of selected catalysts in the future.

Early works have reported the kinetics and reaction mechanisms of zeolite formation and conversion by *in situ* time-resolved SXRD, notably by Norby and co-workers.[99–104] They include the hydrothermal conversion of **LTA** zeolite[99], the migration of Cs^+ and Na^+ ions in Cs- and Na-Y zeolites by dehydration[105], hydroxysodalite formation[103] and the change in unit cell parameters of Na-Y by hydrofluorocarbon-134 adsorption[104], etc. The time-resolved structural transformation of boron-substituted-ZSM-5 into the β-cristobalite phase has also been studied.[106] The migration of Cs^+ ions in a much lower symmetry ZSM-5 as a function of temperature has been reported by Mentzen et al.[107]

Owing to the optimisation of the modern SXRD instrumental set-up, *in situ* SXRD experiments that are more closely related to catalysis chemistry have recently been carried out. For example, Wragg et al. have studied the SAPO-34 zeolite catalyst during the methanol-to-olefins (MTO) process under reaction condition, in combination with Raman and mass spectroscopic techniques.[108] Anisotropic changes in the unit cell parameters have been observed during the process. It is related to the formation of reaction intermediates (the hydrocarbon pool, HCP), and the deactivation of SAPO-34. A time-resolved unit cell expansion by 0.5% in volume upon methanol adsorption in SAPO-34, but a contraction by 2% upon water adsorption, measured by *in situ* SXRD have been reported.[55] These changes in unit cell volume have been associated with the size of the adsorbate species, and the strength of interactions with the zeolite framework. Wragg et al. further compared the changes in lattice parameters and occupancies during the MTO process on SAPO-18 and SAPO-34, where over thousands of diffraction patterns were simultaneously processed[109]; this would not be practical and thinkable in the past. High-energy *operando* SXRD study using a 4-mm diameter tube reactor using the one-dimensional Z-scan method has been reported by Wragg et al. (see Figure 17).[110] The tube reactor was scanned along the *z*-axis at a rate of 0.5 mm s^{-1}, with SXRD patterns collected every second. A spatiotemporal variation has been observed within the tube reactor; a new kinetic model for the MTO process is hence proposed. It involves the initial formation of HCP, its subsequent accumulation, followed by the formation of large coke species, and eventually causing catalyst deactivation.

Subsequently, the same group developed this one-dimensional Z-scan method into SXRD-computed tomographic reconstruction mapping, giving a related three-dimensional approach to study the MTO process over SAPO-34.[111] This allows a three-dimensional study of the structural change of the catalyst. It is related to coke formation and catalyst deactivation. It is found that the *c*-axis of the catalyst shows small variations in the degree of deactivation, which also depends on the silicon content of the catalyst. Also, the MTH (methanol-to-hydrocarbons) process over H-ZSM-22 has been recently probed in a similar manner.[112] Alternatively, by the SXRD imaging technique, the intergrowth structure and Al zoning of a ZSM-5 crystal have been studied *in situ* by Beale, Weckhuysen et al. (see Figure 18).[113] Readers may refer to the review article by Beale et al. for more information on the use of the SXRD-based imaging techniques in the *in situ* characterisation of various functional materials.[114]

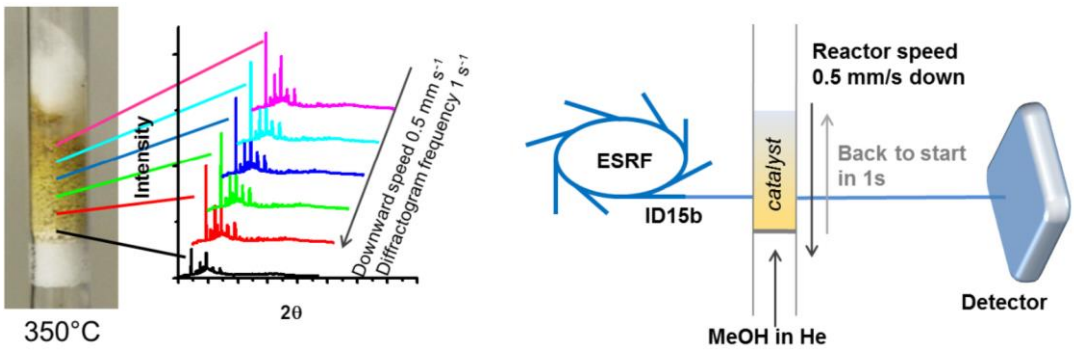

Figure 16. Rietveld-derived tomographic study. Data collection from a large fixed-bed tube reactor using the Z-scan method by Wragg et al., with permission for reproduction.[110]

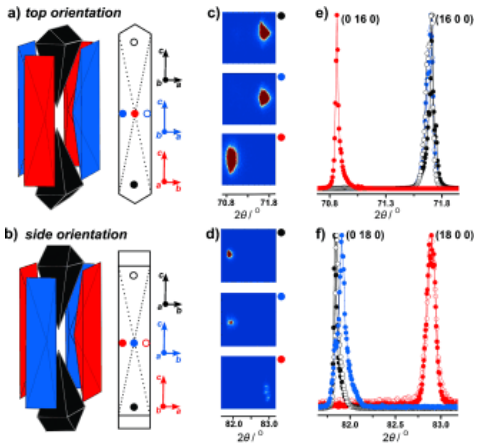

Figure 17. Crystallographic analysis of the intergrowth structure of a single zeolite ZSM-5 crystal by Beale, Weckhuysen et al., with permission for reproduction.[113] (**a**, **b**) ZSM-5 crystal intergrowth (left) and scheme of the colour-coded regions for which the diffraction response was recorded (right) in *top* (**a**) and *side* (**b**) orientations. The crystallographic orientation of each subunit is indicated by the colour-coded vectors. (**c**, **d**) Corresponding diffraction patterns on the 2D detector for the colour-coded spots; for clarity, the patterns are intentionally rotated by 90°. (**e**, **f**) Corresponding normalised X-ray diffractograms, presented for fulfilled Bragg conditions of designated reflections.

Aside from the kinetic and dynamic studies, critical mechanistic information during catalytic reactions can also be obtained. For example, it is accepted that the first step of these catalytic methanol conversion processes is the formation of dimethyl ether via acid-catalysed dehydration. However, how the DME is formed remains debatable. Lo et al. monitored the catalytic conversion of methanol in H-ZSM-5 using *in situ* SXRD in combination with mass spectroscopy (see Figure 18). As seen in Table 1, it has been verified with periodic DFT calculations that the atomic positions of adsorbed methanol species within the H-ZSM-5 framework. Dimethyl ether is formed via a concerted associative mechanism at the low reaction temperature (below 200 °C). The formation mechanism of the HCP intermediate species has also been postulated. [unpublished work] It is therefore envisaged that the *in situ* and *operando* measurements can provide useful information mainly for the catalysis community, who can benefit from the kinetic and dynamic catalytic information, such as the catalytic activity-structure relationship to improve and design various catalytic systems.

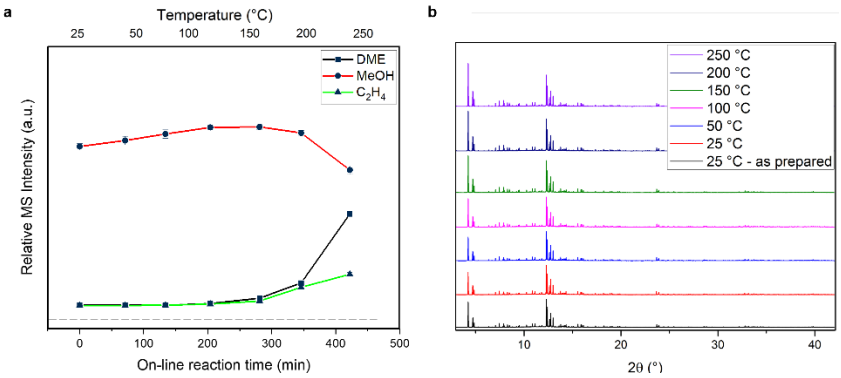

Figure 18. On-line synchrotron X-ray powder diffraction (SXRD) and mass spectrometry, with a flowing stream of methanol vapour over H-ZSM-5 (25 to 250 °C). (**a**) On-line mass spectra showing the relative dimethyl ether and methanol concentrations; noticeable concentration of hydrocarbon products have been detected from 200 °C, showing the initiation of the methanol conversion process, and (**b**) SXRD patterns. [unpublished work]

Table 1. Derived interatomic distances comparison from Rietveld refinements and obtained from ab initio molecular dynamics (AIMD) simulations, between the protonated methanol located in the sinusoidal-straight cross-channel region and the framework O18 and O5 atoms. The numbers in the brackets are the estimated standard deviations. [unpublished work]

Temperature (°C)	**Interatomic distances from Rietveld refinements (Å)**		**Site occupancy of MeOH1**	**Interatomic distances from AIMD simulations (Å)**	
	O18-O_{MeOH1}	O5-O_{MeOH1}	SOF of MeOH1	O18-O_{MeOH1}	O5-O_{MeOH1}
25	3.71(3)	3.74(3)	0.665(4)	3.85	3.75
50	3.72(3)	3.83(3)	0.693(4)	3.95	3.95
100	3.63(3)	3.76(3)	0.581(4)	3.95	4.05
150	3.41(4)	3.68(4)	0.583(4)	3.45	3.55
200	3.40(4)	3.43(4)	0.505(4)	3.45	3.55
250	3.39(4)	3.45(4)	0.457(5)	3.35	3.55

6. *State-of-the-art* development

Recently, beamline BL36XU in SPring-8 (see Figure 19, commissioned since 2013) is specially designed with a nano-sized synchrotron X-ray beam, and equipped with instrumentations capable of performing advanced X-ray absorption fine structure measurements (*in situ*/time-resolved/spatially resolved), laminography, XRD, near ambient pressure hard X-ray photoelectron spectroscopy simultaneously. This beamline initially targets at the study of nano-sized cathode materials for a polymer electrolyte fuel cell (PEFC).[115, 116] For example, the active Pt species in PEFC can be mapped.[117] Using such experimental set-up, some significant challenges in thoroughly and fundamentally understanding the chemistry of various zeolite catalysed reactions may be genuinely tackled.

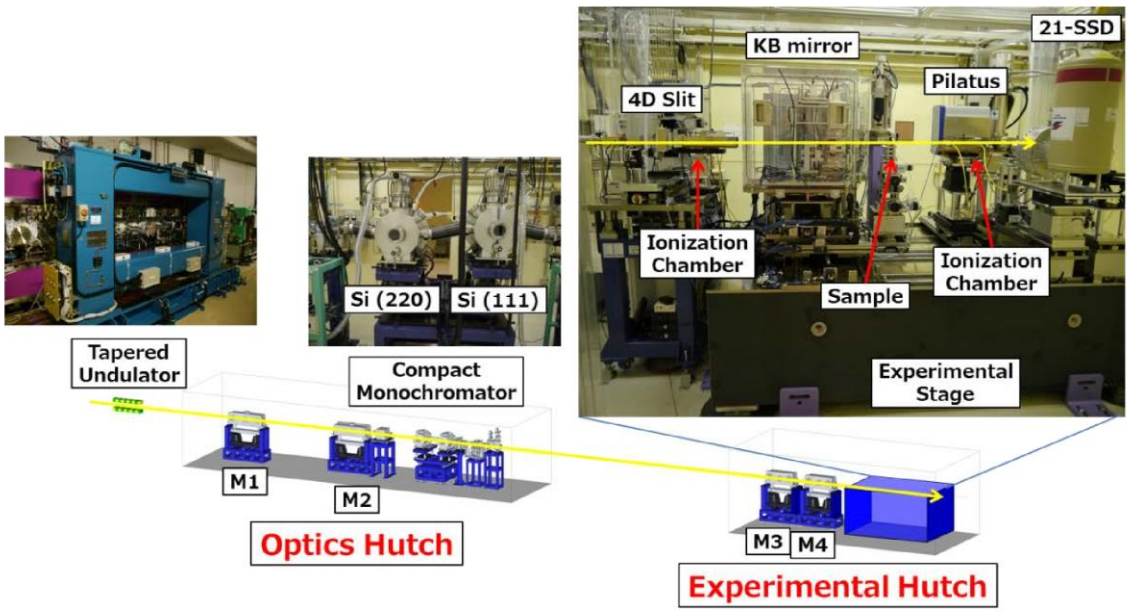

Figure 19. Layout of beamline BL36XU in SPring-8 (Japan) with permission for reproduction.[115]

The *in situ* and *operando* SXRD studies discussed above were performed in a second/hour timescale. However, some study requires much longer time to perform (in terms of weeks to years) under specific conditions, e.g. for zeolite structural stability, geochemical process, catalyst lifetime studies, etc. A novel long-duration SXRD facility has been recently built and commissioned on Beamline I11 in Diamond (see Figure 20).[118] Typically, an SXRD measurement or selected diffraction peak is collected weekly, with the sample being placed in the working reaction environment. With the specially designed features in the experimental hutch, it can accommodate up to 20 different long-duration cells working in parallel. It is shown that microporous NOTT-300 (a metal-organic framework material) can reversibly capture SO_2 and remain highly crystalline for up to 37 weeks.[118] It is believed that this *in situ* gas loading can be broadly applied into the gas storage study of zeolites, and further expand to other exciting materials, such as for battery cycling in a long-duration manner.

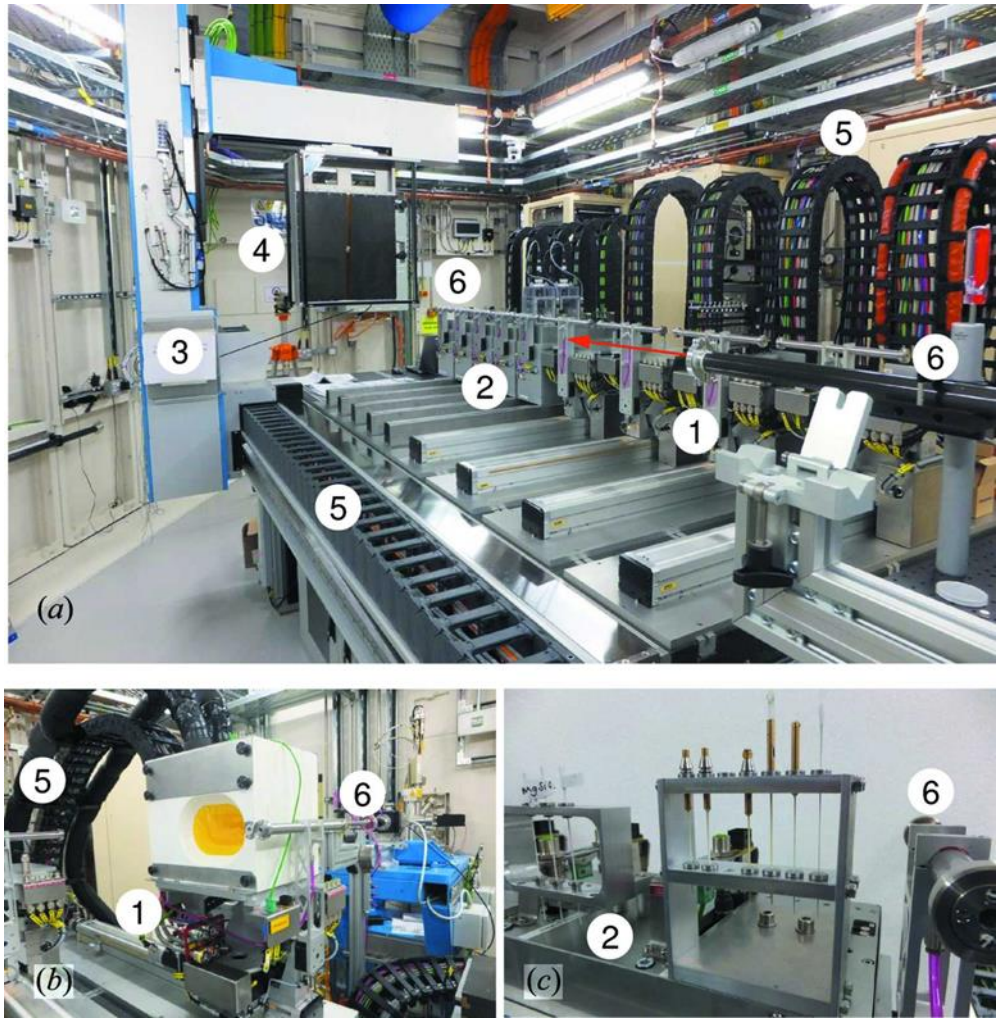

Figure 20. Photographs of the long-duration SXRD experiment facility in Beamline I11 at Diamond (UK) with permission for reproduction[118]: (**a**) key components on the large granite table, (**b**) a low-temperature mineralisation cell and (**c**) capillary samples on a small rack. The key features are labelled as (1) medium stages, (2) small stages, (3) large *XYZ* frame, (4) Pixium area detector, (5) energy (electrical) chains and (6) beam-pipes.

7 Conclusion

Synchrotron X-ray powder diffraction on its own merits or in combination with other analytical techniques so far has enabled investigators to efficiently study many functional materials, where zeolites have been selected explicitly in this Review due to their broad scientific interests and high industrial values. The progressive development and extensive application of this technique suggest that there is much more cutting-edge science to be explored when in-depth case studies are carried out. In terms of the zeolite application in gas storage/separation and catalysis, not only the structures of frameworks and active sites can be determined, but the elucidated framework-organic molecule interactions have also begun to unfold some exciting catalytic mechanisms at an atomistic level. The *in situ, operando,* and long-duration experiments further provide crucial kinetic, dynamic and mechanistic information of some industrially significant reactions. Indeed, with the rapid advances in the modern synchrotron technology and instrumentation, the full capability of this powder diffraction technique in structural determination has yet been truly exploited. More experiments will be designed for interesting materials and associated catalysis chemistry to be unveiled in short future.

8 Acknowledgements

The authors wish to thank EPSRC (UK) and Diamond Light Source Ltd (UK) for financial support of some of the collaborative works with Professor Chiu Tang of beamline I11 (Diamond) mentioned in this review. We are also grateful to the Office of China Postdoctoral Council to grant a fellowship to L. Ye to work at Oxford.

8 References

1. Stöcker, M. (1999). Methanol-to-hydrocarbons: catalytic materials and their behavior. *Microporous Mesoporous Mater.*, *29*(1–2), 3–48.

2. Haag, W. O., Lago, R. M., and Weisz, P. B. (1984). The active site of acidic aluminosilicate catalysts. *Nature*, *309*(5969), 589–591.

3. Gies, H., and Marker, B. (1992). The structure-controlling role of organic templates for the synthesis of porosils in the systems SiO 2/template/H 2 O. *Zeolites*, *12*(1), 42–49.

4. First, E. L., Gounaris, C. E., Wei, J., and Floudas, C. A. (2011). Computational characterization of zeolite porous networks: an automated approach. *Phys. Chem. Chem. Phys.*, *13*(38), 17339–17358.

5. Chester, W., and Derouane, E. G. (2009). *Zeolite Characterization and Catalysis - A Tutorial*. Springer.

6. Jae, J., Tompsett, G. A., Foster, A. J., Hammond, K. D., Auerbach, S. M., Lobo, R. F., and Huber, G. W. (2011). Investigation into the shape selectivity of zeolite catalysts for biomass conversion. *J. Catal.*, *279*(2), 257–268.

7. Reed, T. B., and Breck, D. W. (1956). Crystalline zeolites. II. Crystal structure of synthetic zeolite, type A. *J. Am. Chem. Soc.*, *78*(23), 5972–5977.

8. De Lucas, a., Valverde, J. L., Dorado, F., Romero, a., and Asencio, I. (2005). Influence of the ion exchanged metal (Cu, Co, Ni and Mn) on the selective catalytic reduction of NO X over mordenite and ZSM-5. *J. Mol. Catal. A Chem.*, *225*(1), 47–58.

9. Meier, W. M. (1961). The crystal structure of mordenite (ptilolite). *Zeitschrift für Krist. Mater.*, *115*(1–6), 439–450.

10. Olson, D. H., and Dempsey, E. (1969). The crystal structure of the zeolite hydrogen faujasite. *J. Catal.*, *13*(2), 221–231.

11. Kokotailo, G. T., Lawton, S. L., and Olson, D. H. (1978). Structure of synthetic zeolite ZSM-5. *Nature*, *272*, 437–438.

12. Cejka, J., Corma, A., and Zones, S. (2010). *Zeolites and catalysis: synthesis, reactions and applications*. John Wiley & Sons.

13. Jablonski, G. A., Sand, L. B., and Gard, J. A. (1986). Synthesis and identification of ZSM-5ZSM-11 pentasil intergrowth structures. *Zeolites*, *6*(5), 396–402.

14. Thomas, J. M., and Millward, G. R. (1982). Direct, real-space determination of intergrowths in ZSM-5/ZSM-11 catalysts. *J. Chem. Soc. Chem. Commun.*, (24), 1380–1383.

15. Sławiński, W. A., Wragg, D. S., Akporiaye, D., and Fjellvåg, H. (2014). Intergrowth structure modelling in silicoaluminophosphate SAPO-18/34 family. *Microporous Mesoporous Mater.*, *195*, 311–318.

16. Smith, R. L., Sławiński, W. A., Lind, A., Wragg, D. S., Cavka, J. H., Arstad, B., Fjellvåg, H., Attfield, M. P., Akporiaye, D., and Anderson, M. W. (2015). Nanoporous intergrowths: how crystal growth dictates phase composition and hierarchical structure in the CHA/AEI system. *Chem. Mater.*, *27*(12), 4205–4215.

17. Eikenberry, E. F., Brönnimann, C., Hülsen, G., Toyokawa, H., Horisberger, R., Schmitt, B., Schulze-Briese, C., and Tomizaki, T. (2003). PILATUS: a two-dimensional X-ray detector for

macromolecular crystallography. *Nucl. Instruments Methods Phys. Res. Sect. A Accel. Spectrometers, Detect. Assoc. Equip.*, *501*(1), 260–266.

18. Cockcroft, J. K., and Fitch, A. N. (2008). Experimental setups. In *Powder Diffr.* (pp. 20–57).

19. O'Brien, M. G., Beale, A. M., Jacques, S. D. M., Di Michiel, M., and Weckhuysen, B. M. (2011). Closing the operando gap: The application of high energy photons for studying catalytic solids at work. *Appl. Catal. A Gen.*, *391*(1–2), 468–476.

20. Yabashi, K. T. and T. T. and Y. I. and T. S. and T. K. and K. O. and H. O. and H. K. and S. T. and K. T. and H. T. and S. G. and T. I. and M., Tono, K., Togashi, T., Inubushi, Y., Sato, T., Katayama, T., Ogawa, K., Ohashi, H., Kimura, H., Takahashi, S., and Takeshita, K. (2013). Beamline, experimental stations and photon beam diagnostics for the hard x-ray free electron laser of SACLA. *New J. Phys.*, *15*(8), 83035.

21. Sá, J., and Szlachetko, J. (2014). Heterogeneous Catalysis Experiments at XFELs. Are we Close to Producing a Catalysis Movie? *Catal. Letters*, *144*(2), 197–203.

22. Young, R. A. (1993). *The Rietveld method* (Vol. 5).

23. David, W. I. F. (2002). *Structure determination from powder diffraction data* (Vol. 13). Oxford University Press on Demand.

24. David, W. I. F. I. F. (2004). Powder diffraction: least-squares and beyond. *J. Res. Natl. Inst. Stand. Technol.*, *109*(1), 107.

25. Coleman, J. N., Lotya, M., O'Neill, A., Bergin, S. D., King, P. J., Khan, U., Young, K., Gaucher, A., De, S., Smith, R. J., Shvets, I. V, Arora, S. K., Stanton, G., Kim, H.-Y., Lee, K., Kim, G. T., Duesberg, G. S., Hallam, T., Boland, J. J., Wang, J. J., Donegan, J. F., Grunlan, J. C., Moriarty, G., Shmeliov, A., Nicholls, R. J., Perkins, J. M., Grieveson, E. M., Theuwissen, K., McComb, D. W., Nellist, P. D., and Nicolosi, V. (2011). Two-dimensional nanosheets produced by liquid exfoliation of layered materials. *Science*, *331*(6017), 568–71.

26. Lutterotti, L., and Scardi, P. (1990). Simultaneous structure and size–strain refinement by the Rietveld method. *J. Appl. Crystallogr.*, *23*(4), 246–252.

27. McCusker, L. B. (1991). Zeolite crystallography. Structure determination in the absence of conventional single-crystal data. *Acta Crystallogr. Sect. A*, *47*(4), 297–313.

28. Sastre, G., Vidal-Moya, J. A., Blasco, T., Rius, J., Jordá, J. L., Navarro, M. T., Rey, F., and Corma, A. (2002). Preferential Location of Ge Atoms in Polymorph C of Beta Zeolite (ITQ-17) and Their Structure-Directing Effect: A Computational, XRD, and NMR Spectroscopic Study. *Angew. Chem. Int. Ed.*, *41*(24), 4722–4726.

29. Yun, Y., Zou, X., Hovmöller, S., and Wan, W. (2015). Three-dimensional electron diffraction as a complementary technique to powder X-ray diffraction for phase identification and structure solution of powders. *IUCrJ*, *2*(2), 267–282.

30. McCusker, L. B. (1988). The ab initio structure determination of Sigma-2 (a new clathrasil phase) from synchrotron powder diffraction data. *J. Appl. Crystallogr.*, *21*(4), 305–310.

31. McCusker, L. B. (1988). The ab initio structure determination of Sigma-2 (a new clathrasil phase) from synchrotron powder diffraction data. *J. Appl. Crystallogr.*, *21*(4), 305–310.

32. McCusker, L. B., Baerlocher, C., Grosse-Kunstleve, R., Brenner, S., and Wessels, T. (2001). Solving complex zeolite structures from powder diffraction data. *Chim. Int. J. Chem.*, *55*(6), 497–504.

33. Fyfe, C. A., Gies, H., Kokotailo, G. T., Pasztor, C., Strobl, H., and Cox, D. E. (1989). Detailed investigation of the lattice structure of zeolite ZSM-11 by a combination of solid-state NMR and synchrotron x-ray diffraction techniques. *J. Am. Chem. Soc.*, *111*(7), 2470–2474.

34. Corma, A., Diaz-Cabanas, M. J., Jorda, J. L., Rey, F., Sastre, G., and Strohmaier, K. G. (2008). A zeolitic structure (ITQ-34) with connected 9-and 10-ring channels obtained with phosphonium cations as structure directing agents. *J. Am. Chem. Soc.*, *130*(49), 16482–16483.

35. Sun, J., Bonneau, C., Cantín, A., Corma, A., Díaz-Cabañas, M. J., Moliner, M., Zhang, D., Li, M., and Zou, X. (2009). The ITQ-37 mesoporous chiral zeolite. *Nature*, *458*(7242), 1154–7.

36. Breck, D. W. (1974). Zeolites molecular sieves, chemistry and use. Wiley, New York.

37. Wilson, S., and Barger, P. (1999). The characteristics of SAPO-34 which influence the conversion of methanol to light olefins. *Microporous Mesoporous Mater.*, *29*(1–2), 117–126.

38. Lok, B. M., Messina, C. A., Patton, R. L., Gajek, R. T., Cannan, T. R., and Flanigen, E. M. (1984). Silicoaluminophosphate molecular sieves: another new class of microporous crystalline inorganic solids. *J. Am. Chem. Soc.*, *106*(20), 6092–6093.

39. Wilson, S. T., Lok, B. M., Messina, C. A., Cannan, T. R., and Flanigen, E. M. (1982). Aluminophosphate molecular sieves: a new class of microporous crystalline inorganic solids. *J. Am. Chem. Soc.*, *104*(4), 1146–1147.

40. Dinnebier, R. E., and Billinge, S. J. L. (2008). *Powder Diffraction - Theory and Practice*.

41. Willmott, P. (2011). *An introduction to synchrotron radiation: techniques and applications*. John Wiley & Sons.

42. Bragg, W. L. (1913). The structure of some crystals as indicated by their diffraction of X-rays. In *Proc. R. Soc. London A Math. Phys. Eng. Sci.* (Vol. 89, pp. 248–277). The Royal Society.

43. Rietveld, H. M. (1993). *The Rietveld Method*. *Oxford Univ. Press*. Oxford University Press.

44. Le Bail, A. (1995). Modelling the silica glass structure by the Rietveld method. *J. Non. Cryst. Solids*, *183*(1–2), 39–42.

45. Parker, J. E., Thompson, S. P., Cobb, T. M., Yuan, F., Potter, J., Lennie, A. R., Alexander, S., Tighe, C. J., Darr, J. a., Cockcroft, J. C., and Tang, C. C. (2011). High-throughput powder diffraction on beamline I11 at Diamond. *J. Appl. Crystallogr.*, *44*(1), 102–110.

46. Thompson, S. P., Parker, J. E., Marchal, J., Potter, J., Birt, A., Yuan, F., Fearn, R. D., Lennie, A. R., Street, S. R., and Tang, C. C. (2011). Fast X-ray powder diffraction on I11 at Diamond. *J. Synchrotron Radiat.*, *18*(4), 637–648.

47. Coelho, A. A. (2000). Whole-profile structure solution from powder diffraction data using simulated annealing. *J. Appl. Crystallogr.*, *33*(3), 899–908.

48. Larson, A. C., and Von Dreele, R. B. (1994). Gsas. *Gen. Struct. Anal. Syst. LANSCE, MS-H805, Los Alamos, New Mex.*

49. Thompson, P., Cox, D. E., and Hastings, J. B. (1987). Rietveld Refinement of Debye-Scherrer Synchrotron X-ray Data from Al2O3. *J. Appl. Crystallogr.*, *20*(2), 79–83.

50. Lo, B. T. W., Ye, L., Qu, J., Sun, J., Zheng, J., Kong, D., Murray, C. A., Tang, C. C., and Tsang, S. C. E. (2016). Elucidation of Adsorbate Structures and Interactions on Brønsted Acid Sites in H-ZSM-5 by Synchrotron X-ray Powder Diffraction. *Angew. Chem. Int. Ed.*, *55*(20), 5981–5984.

51. Østbø, N. P. P., Goyal, R., Jobic, H., and Fitch, A. N. N. (1999). The location of pyridine in sodium–silver–Y zeolite by powder synchrotron X-ray diffraction. *Microporous mesoporous Mater.*, *30*(2), 255–265.

52. Ye, L., Lo, B. T. W., Qu, J., Wilkinson, I., Hughes, T., Murray, C. A., Tang, C. C., and Tsang, S. C. E. (2016). Probing atomic positions of adsorbed ammonia molecules in zeolite, *52*(16), 3422–3425.

53. Teixeira, I. F., Lo, B. T. W., Kostetskyy, P., Stamatakis, M., Ye, L., Tang, C. C., Mpourmpakis, G., and Tsang, S. C. E. (2016). From Biomass-Derived Furans to Aromatics with Ethanol over Zeolite. *Angew. Chem. Int. Ed.*, *55*(42), 13061–13066.

54. Tsang, E. S. C., Ye, L., Lo, B., Song, Q., Zheng, J., Kong, D., and Tang, C. (2017). A New Route for De-carboxylation of Lactones over Zn/ZSM-5: Elucidation of Structure and Molecular Interactions. *Angew. Chem. Int. Ed.*, *56*(36), 10711–10716.

55. Wragg, D. S., Johnsen, R. E., Norby, P., and Fjellvag, H. (2010). The adsorption of methanol and water on SAPO-34: in situ and ex situ X-ray diffraction studies. *Microporous Mesoporous Mater.*, *134*(1–3), 210–215.

56. Mentzen, B. F. (1989). Localizing adsorption sites in zeolitic materials by X-ray powder diffraction: pyridine sorbed in B. ZSM-5. *J. Appl. Crystallogr.*, *22*(2), 100–104.

57. Mentzen, B. F. (1987). Characterization of guest molecules adsorbed on zeolites of known structure by combined x-ray powder profile refinements and conventional difference-fourier techniques. Part II-Localization of the n-hexane, TPA and p-xylene guests in a pentasil type zeoli. *Mater. Res. Bull.*, *22*(4), 489–496.

58. Arletti, R., Martucci, A., Alberti, A., Pasti, L., Nassi, M., and Bagatin, R. (2012). Location of MTBE and toluene in the channel system of the zeolite mordenite: Adsorption and host–guest interactions. *J. Solid State Chem.*, *194*, 135–142.

59. Smeets, S., and McCusker, L. B. (2017). Location of Organic Structure-Directing Agents in Zeolites Using Diffraction Techniques. In *Struct. Bond.* (pp. 1–31). Berlin, Heidelberg: Springer Berlin Heidelberg.

60. Pinar, A. B., Gómez-Hortigüela, L., McCusker, L. B., and Pérez-Pariente, J. (2013). Controlling the aluminum distribution in the zeolite ferrierite via the organic structure directing agent. *Chem. Mater.*, *25*(18), 3654–3661.

61. Dědeček, J., Sobalík, Z., and Wichterlová, B. (2012). Siting and Distribution of Framework Aluminium Atoms in Silicon-Rich Zeolites and Impact on Catalysis. *Catal. Rev.*, *54*(2), 135–223.

62. Martucci, A., Cruciani, G., Alberti, A., Ritter, C., Ciambelli, P., and Rapacciuolo, M. (2000). Location of Brønsted sites in D-mordenites by neutron powder diffraction. *Microporous Mesoporous Mater.*, *35*, 405–412.

63. Czjzek, M., Jobic, H., Fitch, A. N., and Vogt, T. (1992). Direct Determination of Proton Positions in D-Y and H-Y Zeolite Samples by Neutron Powder Diffraction. *J. Phys. Chem.*, *96*(1), 1535–1540.

64. Czjzek, M., Vogt, T., and Fuess, H. (1989). Location of para-Xylene in Yb-Faujasite (Zeolite Y) by Neutron Diffraction. *Angew. Chem. Int. Ed.*, *28*(6), 770–772.

65. Goyal, R., Fitch, A. N., and Jobic, H. (2000). Powder neutron and X-ray diffraction studies of benzene adsorbed in zeolite ZSM-5. *J. Phys. Chem. B*, *104*(13), 2878–2884.

66. Bae, T.-H., Hudson, M. R., Mason, J. A., Queen, W. L., Dutton, J. J., Sumida, K., Micklash, K. J., Kaye, S. S., Brown, C. M., and Long, J. R. (2013). Evaluation of cation-exchanged zeolite adsorbents for post-combustion carbon dioxide capture. *Energy Environ. Sci.*, *6*(1), 128–138.

67. Kosinov, N., Gascon, J., Kapteijn, F., and Hensen, E. J. M. (2016). Recent developments in zeolite membranes for gas separation. *J. Memb. Sci.*, *499*, 65–79.

68. Shang, J., Li, G., Singh, R., Gu, Q., Nairn, K. M., Bastow, T. J., Medhekar, N., Doherty, C. M., Hill, A. J., Liu, J. Z., and Webley, P. A. (2012). Discriminative separation of gases by a "molecular trapdoor" mechanism in chabazite zeolites. *J. Am. Chem. Soc.*, *134*(46), 19246–19253.

69. Weitkamp, J., Fritz, M., and Ernst, S. (1995). Zeolites as media for hydrogen storage. *Int. J. Hydrogen Energy*, *20*(12), 967–970.

70. Langmi, H. W., Book, D., Walton, A., Johnson, S. R., Al-Mamouri, M. M., Speight, J. D., Edwards, P. P., Harris, I. R., and Anderson, P. A. (2005). Hydrogen storage in ion-exchanged zeolites. *J. Alloys Compd.*, *404*, 637–642.

71. Dong, J., Wang, X., Xu, H., Zhao, Q., and Li, J. (2007). Hydrogen storage in several microporous zeolites. *Int. J. Hydrogen Energy*, *32*(18), 4998–5004.

72. Yang, Z., Xia, Y., and Mokaya, R. (2007). Enhanced Hydrogen Storage Capacity of High Surface Area Zeolite-like Carbon Materials. *J. Am. Chem. Soc.*, *129*(6), 1673–1679.

73. Doonan, C. J., Tranchemontagne, D. J., Glover, T. G., Hunt, J. R., and Yaghi, O. M. (2010). Exceptional ammonia uptake by a covalent organic framework. *Nat. Chem.*, *2*(3), 235–238.

74. Rodriguez-Santiago, L., Sierka, M., Branchadell, V., Sodupe, M., and Sauer, J. (1998). Coordination of Cu+ ions to zeolite frameworks strongly enhances their ability to bind NO2: An ab initio density functional study. *J. Am. Chem. Soc.*, *120*(7), 1545–1551.

75. Mentzen, B. F., and Bergeret, G. (2007). Crystallographic Determination of the Positions of the Copper Cations in Zeolite MFI. *J. Phys. Chem. C*, *111*(111), 12512–12516.

76. Weitkamp, J., and Puppe, L. (2013). *Catalysis and zeolites: fundamentals and applications*. Springer Science & Business Media.

77. Öhman, L.-O., Ganemi, B., Björnbom, E., Rahkamaa, K., Keiski, R. L., and Paul, J. (2002). Catalyst preparation through ion-exchange of zeolite Cu-, Ni-, Pd-, CuNi-and CuPd-ZSM-5. *Mater. Chem. Phys.*, *73*(2), 263–267.

78. Beale, A. M., Lezcano-Gonzalez, I., Slawinksi, W. A., and Wragg, D. S. (2016). Correlation between Cu ion migration behaviour and deNO x activity in Cu-SSZ-13 for the standard NH 3-SCR reaction. *Chem. Commun.*, *52*(36), 6170–6173.

79. Lezcano-Gonzalez, I., Wragg, D. S., Slawinski, W. A., Hemelsoet, K., Van Yperen-De Deyne, A., Waroquier, M., Van Speybroeck, V., and Beale, A. M. (2015). Determination of the Nature of the Cu Coordination Complexes Formed in the Presence of NO and NH3 within SSZ-13. *J. Phys. Chem. C*, *119*(43), 24393–24403.

80. Ono, Y. (1992). Transformation of Lower Alkanes Into Aromatic-Hydrocarbons Over Zsm-5 Zeolites. *Catal. Rev. Eng.*, *34*(June), 179–226.

81. Ratnasamy, P., Singh, A. P., and Sharma, S. (1996). Halogenation over zeolite catalysts. *Appl. Catal. A Gen.*, *135*(1), 25–55.

82. Mentzen, B. F. (2007). Crystallographic determination of the positions of the monovalent H, Li, Na, K, Rb, and Tl cations in fully dehydrated MFI type zeolites. *J. Phys. Chem. C*, *111*(51), 18932–18941.

83. Hensen, E. J. M., Pidko, E. A., Rane, N., and van Santen, R. A. (2007). Water-Promoted Hydrocarbon Activation Catalyzed by Binuclear Gallium Sites in ZSM-5 Zeolite. *Angew. Chem. Int. Ed.*, *46*(38), 7273–7276.

84. Long, J., Wang, X., Zhang, G., Dong, J., Yan, T., Li, Z., and Fu, X. (2007). A mononuclear cyclopentadiene–iron complex grafted in the supercages of HY zeolite: synthesis, structure, and reactivity. *Chem. Eur. J.*, *13*(28), 7890–7899.

85. Frising, T., and Leflaive, P. (2008). Extraframework cation distributions in X and Y faujasite zeolites: A review. *Microporous Mesoporous Mater.*, *114*(1–3), 27–63.

86. Pidko, E. A., Hensen, E. J. M., and Van Santen, R. A. (2012). Self-organization of extraframework cations in zeolites. In *Proc. R. Soc. A* (Vol. 468, pp. 2070–2086). The Royal Society.

87. Smith, J. V. (1971). Faujasite-type structures: aluminosilicate framework: positions of cations and molecules: nomenclature. In *Mol. Sieve Zeolites-I* (pp. 171–200). ACS Publications.

88. Mortier, W. J. (1982). *Compilation of extra framework sites in zeolites*. Butterworth Scientific Limited on behalf of the Structure Commission of the International Zeolite Association.

89. Corma, A., Fornes, V., and Rey, F. (1990). Extraction of extra-framework aluminium in ultrastable Y zeolites by (NH4) 2SiF6 treatments: I. physicochemical characterization. *Appl. Catal.*, *59*(1), 267–274.

90. DeCanio, S. J., Sohn, J. R., Fritz, P. O., and Lunsford, J. H. (1986). Acid catalysis by dealuminated zeolite-Y: I. Methanol dehydration and cumene dealkylation. *J. Catal.*, *101*(1), 132–141.

91. Beyerlein, R. A., McVicker, G. B., Yacullo, L. N., and Ziemiak, J. J. (1988). The influence of framework and nonframework aluminum on the acidity of high-silica, proton-exchanged FAU-framework zeolites. *J. Phys. Chem.*, *92*(7), 1967–1970.

92. Sohn, J. R., DeCanio, S. J., Fritz, P. O., and Lunsford, J. H. (1986). Acid catalysis by dealuminated zeolite Y. 2. The roles of aluminum. *J. Phys. Chem.*, *90*(20), 4847–4851.

93. Sanz, J., Fornés, V., and Corma, A. (1988). Extraframework aluminium in steam-and SiCl 4-dealuminated Y zeolite. A 27 Al and 29 Si nuclear magnetic resonance study. *J. Chem. Soc. Faraday Trans. 1 Phys. Chem. Condens. Phases*, *84*(9), 3113–3119.

94. Li, S., Zheng, A., Su, Y., Zhang, H., Chen, L., Yang, J., Ye, C., and Deng, F. (2007). Brønsted / Lewis Acid Synergy in Dealuminated HY Zeolite : A Combined Solid-State NMR and Theoretical Calculation Study. *J. Am. Chem. Soc.*, *129*(12), 11161–11171.

95. Agostini, G., Lamberti, C., Palin, L., Milanesio, M., Danilina, N., Xu, B., Janousch, M., and van Bokhoven, J. A. (2009). In situ XAS and XRPD parametric Rietveld refinement to understand dealumination of Y zeolite catalyst. *J. Am. Chem. Soc.*, *132*(2), 667–678.

96. Ye, L., Teixeira, I. F., Lo, B. T., Zhao, P., and Tsang, E. (2017). Spatial Differentiation of Brønsted Acid Sites by Probe Molecule in Zeolite USY using Synchrotron X-ray Powder Diffraction. *Chem. Commun.*, *53*(1), 9725–9728.

97. Deka, U., Juhin, A., Eilertsen, E. A., Emerich, H., Green, M. A., Korhonen, S. T., Weckhuysen, B. M., and Beale, A. M. (2012). Confirmation of isolated Cu 2+ ions in SSZ-13

zeolite as active sites in NH 3-selective catalytic reduction. *J. Phys. Chem. C*, *116*(7), 4809–4818.

98. Norby, P. (1995). In-situ time resolved synchrotron powder diffraction studies of synthesis and chemical reactions. *Mater. Sci. Forum*, *228*(1), 147–152.

99. Norby, P. (1997). Hydrothermal conversion of zeolites: an in situ synchrotron X-ray powder diffraction study. *J. Am. Chem. Soc.*, *119*(22), 5215–5221.

100. Christensen, A. N., Norby, P., and Hanson, J. C. (1997). In-situ investigation of magnesium aluminophosphate synthesis by synchrotron X-ray powder diffraction. *Acta Chem. Scand.*, *51*(3), 249–258.

101. Norby, P. (1997). Synchrotron powder diffraction using imaging plates: crystal structure determination and Rietveld refinement. *J. Appl. Crystallogr.*, *30*(1), 21–30.

102. Norby, P. (2006). In-situ XRD as a tool to understanding zeolite crystallization. *Curr. Opin. Colloid Interface Sci.*, *11*(2), 118–125.

103. Gualtieri, A., Norby, P., Artioli, G., and Hanson, J. (1997). Kinetic study of hydroxysodalite formation from natural kaolinites by time-resolved synchrotron powder diffraction. *Microporous Mater.*, *9*(3–4), 189–201.

104. Grey, C. P., Poshni, F. I., Gualtieri, A. F., Norby, P., Hanson, J. C., and Corbin, D. R. (1997). Combined MAS NMR and X-ray Powder Diffraction Structural Characterization of Hydrofluorocarbon-134 Adsorbed on Zeolite NaY: Observation of Cation Migration and Strong Sorbate− Cation Interactions. *J. Am. Chem. Soc.*, *119*(8), 1981–1989.

105. Norby, P., Poshni, F. I., Gualtieri, A. F., Hanson, J. C., and Grey, C. P. (1998). Cation Migration in Zeolites: An in Situ Powder Diffraction and MAS NMR Study of the Structure of Zeolite Cs (Na)− Y during Dehydration. *J. Phys. Chem. B*, *102*(5), 839–856.

106. Leardini, L., Martucci, A., and Cruciani, G. (2013). The unusual thermal behaviour of boron-ZSM-5 probed by “in situ” time-resolved synchrotron powder diffraction. *Microporous Mesoporous Mater.*, *173*, 6–14.

107. Mentzen, B. F., Bergeret, G. G., Emerich, H., and Weber, H.-P. P. (2006). Dehydrated and Cs+-exchanged MFI zeolites: Location and population of Cs+ from in situ diffraction data as a function of temperature and degree of exchange. *J. Phys. Chem. B*, *110*(1), 97–106.

108. Wragg, D. S., Johnsen, R. E., Balasundaram, M., Norby, P., Fjellvåg, H., Grønvold, A., Fuglerud, T., Hafizovic, J., Vistad, Ø. B., and Akporiaye, D. (2009). SAPO-34 methanol-to-olefin catalysts under working conditions: A combined in situ powder X-ray diffraction, mass spectrometry and Raman study. *J. Catal.*, *268*(2), 290–296.

109. Wragg, D. S., Akporiaye, D., and Fjellvåg, H. (2011). Direct observation of catalyst behaviour under real working conditions with X-ray diffraction: Comparing SAPO-18 and SAPO-34 methanol to olefin catalysts. *J. Catal.*, *279*(2), 397–402.

110. Wragg, D. S., O’Brien, M. G., Bleken, F. L., Di Michiel, M., Olsbye, U., and Fjellvãg, H. (2012). Watching the methanol-to-olefin process with time- and space-resolved high-energy operando X-ray diffraction. *Angew. Chem. Int. Ed.*, *51*(32), 7956–7959.

111. Wragg, D. S., O’Brien, M. G., Di Michiel, M., and Lønstad-Bleken, F. (2015). Rietveld analysis of computed tomography and its application to methanol to olefin reactor beds. *J. Appl. Crystallogr.*, *48*, 1719–1728.

112. del Campo, P., Slawinski, W. A., Henry, R., Erichsen, M. W., Svelle, S., Beato, P., Wragg, D.,

and Olsbye, U. (2016). Time- and space-resolved high energy operando X-ray diffraction for monitoring the methanol to hydrocarbons reaction over H-ZSM-22 zeolite catalyst in different conditions. *Surf. Sci.*, *648*, 141–149.

113. Ristanović, Z., Hofmann, J. P., Deka, U., Schülli, T. U., Rohnke, M., Beale, A. M., and Weckhuysen, B. M. (2013). Intergrowth Structure and Aluminium Zoning of a Zeolite ZSM-5 Crystal as Resolved by Synchrotron-Based Micro X-Ray Diffraction Imaging. *Angew. Chem. Int. Ed.*, *52*(50), 13382–13386.

114. Beale, A. M., Jacques, S. D. M., Gibson, E. K., and Di Michiel, M. (2014). Progress towards five dimensional diffraction imaging of functional materials under process conditions. *Coord. Chem. Rev.*, *277*, 208–223.

115. Sekizawa, O., Uruga, T., Takagi, Y., Nitta, K., Kato, K., Tanida, H., Uesugi, K., Hoshino, M., Ikenaga, E., and Takeshita, K. (2016). SPring-8 BL36XU: Catalytic Reaction Dynamics for Fuel Cells. In *J. Phys. Conf. Ser.* (Vol. 712).

116. Sekizawa, O., Uruga, T., Tada, M., Nitta, K., Kato, K., Tanida, H., Takeshita, K., Takahashi, S., Sano, M., and Aoyagi, H. (2013). New XAFS beamline for structural and electronic dynamics of nanoparticle catalysts in fuel cells under operating conditions. In *J. Phys. Conf. Ser.* (Vol. 430, p. 12020). IOP Publishing.

117. Takao, S., Sekizawa, O., Nagamatsu, S., Kaneko, T., Yamamoto, T., Samjeské, G., Higashi, K., Nagasawa, K., Tsuji, T., and Suzuki, M. (2014). Mapping platinum species in polymer electrolyte fuel cells by spatially resolved XAFS techniques. *Angew. Chem. Int. Ed.*, *53*(51), 14110–14114.

118. Murray, C. A., Potter, J., Day, S. J., Baker, A. R., Thompson, S. P., Kelly, J., Morris, C. G., Yang, S., and Tang, C. C. (2017). New synchrotron powder diffraction facility for long-duration experiments. *J. Appl. Crystallogr.*, *50*(1), 172–183.